Spectrochimica Acta Part A: Molecular and Biomolecular Spectroscopy 95 (2012) 382–398

Contents lists available at SciVerse ScienceDirect

Spectrochimica Acta Part A: Molecular and Biomolecular Spectroscopy

journal homepage: www.elsevier.com/locate/saa

# Tetradentate Schiff base ligands and their complexes: Synthesis, structural characterization, thermal, electrochemical and alkane oxidation

Gökhan Ceyhan [a,c], Muhammet Köse [b], Vickie McKee [b], Serhan Uruş [a,c], Ayşegül Gölcü [a], Mehmet Tümer [a,*]

[a] Kahramanmaraş Sütçü Imam University, Chemistry Department, 46100 K. Maras, Turkey
[b] Chemistry Department, Loughborough University, LE11 3TU Leics, UK
[c] Kahramanmaraş Sütçü Imam University, Research and Development Center for University-Industry-Public Relations, 46100 K. Maras, Turkey

ARTICLE INFO

*Article history:*
Received 5 December 2011
Received in revised form 12 March 2012
Accepted 3 April 2012
Available online 21 April 2012

*Keywords:*
Schiff base
X-ray
Alkane oxidation
Electrochemical
Thermal
Oxidized products

ABSTRACT

Three Schiff base ligands ($H_2L^1$–$H_2L^3$) with $N_2O_2$ donor sites were synthesized by condensation of 1,5-diaminonapthalene with benzaldehyde derivatives. A series of Cu(II), Co(II), Ni(II), Mn(II) and Cr(III) complexes were prepared and characterized by spectroscopic and analytical methods. Thermal, electrochemical and alkane oxidation reactions of the ligands and their metal complexes were investigated. Extensive application of 1D ($^1$H, $^{13}$C NMR) and 2D (COSY, HETCOR, HMBC and TOSCY) NMR techniques were used to characterize the structures of the ligands and establish the $^1$H and $^{13}$C resonance assignments of the three ligands. Ligands $H_2L^1$ and $H_2L^3$ were obtained as single crystals from THF solution and characterized by X-ray diffraction. Both molecules are centrosymmetric and asymmetric unit contains one half of the molecule. Catalytic alkane oxidation reactions with the transition metal complexes investigated using cyclohexane and cyclooctane as substrates. The Cu(II) and Cr(III) complexes showed good catalytic activity in the oxidation of cyclohexane and cyclooctane to desired oxidized products. Electrochemical and thermal properties of the compounds were also investigated.



## 1. Introduction

The ortho-hydroxy Schiff bases belong to the group of compounds forming intramolecular hydrogen bonds generating ever growing interest due to π-electron coupling between the acid and base centers [1–4]. Such systems are interesting both from the theoretical and experimental point of view. The intramolecular proton transfer reaction proceeds comparatively easily in these compounds. Intramolecular π-electron coupling leads to the strengthening of the hydrogen bonds in these systems. These compounds are potential materials for molecular memory and optical switch devices [5] or fluorescent probes of biological systems [6].

In Schiff base metal complexes, the environment at the coordination center can be modified by attaching different substituents to the ligand, which provides a useful range of steric and electronic properties essential for the fine-tuning of structure and reactivity. Therefore, Schiff base ligands are among the most fundamental chelating systems in coordination chemistry [7,8] and complexes of both transition and p-block metals based on this type ligands were shown to catalyze a wide variety of reactions [9,10].

The transformation of hydrocarbons into oxygenated compounds has been extensively investigated over the last decades, because the products are valuable intermediates for organic synthesis. Cyclohexane (CyH) oxidation into cyclohexanol (Cy—OH) and cyclohexanone (Cy=O) has a great importance in industry. Over a billion tones of Cy=O and Cy—OH are produced each year and are generally used for the synthesis of Nylon-6 and Nylon-6,6 [11]. A Co-naphthenate complex is used as a catalyst to initiate the radical oxidation of cyclohexane using molecular oxygen from the air at 160 °C and 15 bar pressure. On completion of the reaction, only 4% of CyH is converted to oxidized products and with selectivity towards Cy=O and Cy—OH [11]. Tanase et al. have synthesized polydentate pyridine based ligand and its iron complexes [12]. These complexes were active in the catalytic oxidation of some hydrocarbons, such as cyclohexane and cyclooctane [12,13].

Microwave technology using the green oxidant hydrogen peroxide can reduce the reaction times and energy consumption with an increase in cyclohexane conversion and Cy—OH and Cy=O selectivity [14–16]. We obtained high yields with high conversions in short times, in our previous catalytic oxidation studies with microwave power [15,16]. Carvalho et al. have studied the cyclohexane oxidation under microwave conditions by using Fe(III) complex catalysts, hydrogen peroxide as oxidant and acetonitrile as solvent [17]. Cy—OH, Cy=O and adipic acid were obtained as major products in this study with a good CyH conversion and Cy—OH, Cy=O selectivity. According to the study of Clark et al., the Co-salen complex has shown a good catalytic activity for the oxidation of cyclohexene to 2-cyclohexen-1-ol, cyclohexene oxide and cyclohanediol with $H_2O_2$ under 300 W microwave power [14].

* Corresponding author. Tel.: +90 344 2191093; fax: +90 344 2191042.
*E-mail address:* mtumer@ksu.edu.tr (M. Tümer).

1386-1425/$ - see front matter © 2012 Elsevier B.V. All rights reserved.
http://dx.doi.org/10.1016/j.saa.2012.04.001

In this paper, we report the synthesis and characterization of three Schiff base ligands ($H_2L^1$ = *N*,*N*′-bis[3-hydroxy salicylidene]-1,5-diamino naphthalene, $H_2L^2$ = *N*,*N*′-bis[4-hydroxy salicylidene]-1,5-diamino naphthalene and $H_2L^3$ = *N*,*N*′-bis[3-methoxy salicylidene]-1,5-diamino naphthalene) and their transition metal complexes. The catalytic activity of the Cu(II), Co(II), Cr(III), Ni(II) and Mn(II) complexes were investigated and the Cu(II) and Cr(III) complexes showed enhanced catalytic effects for oxidation reactions under microwave conditions using $H_2O_2$ as oxidant. The structural characterization of the ligands $H_2L^1$ and $H_2L^1$ were done by single crystal X-ray diffraction. The 1D ($^1$H, $^{13}$C NMR) and 2D (COSY, HETCOR, HMBC and TOCSY) NMR techniques were used for characterization of the structures of the ligands.

## 2. Experimental

### 2.1. Materials and measurements

All reagents and solvents were of reagent-grade quality and obtained from commercial suppliers (Aldrich or Merck). Elemental analyses (C, H, N) were performed using a LECO CHNS 932. Infrared spectra were obtained using KBr discs (4000–400 $cm^{-1}$) on a Perkin Elmer Spectrum 100 FT-IR. Far IR spectra of the complexes were recorded on a Perkin Elmer spectrum 400 FT-IR/FT-FAR. Electronic spectra in the 200–900 nm range were obtained on a Perkin Elmer Lambda 45 spectrophotometer. Molar conductances of the Schiff base ligands and their transition metal complexes were determined in DMF ($\sim 10^{-3}$ M) at room temperature using a Jenway Model 4070 conductivity meter. Magnetic measurements were carried out by the Gouy method using $Hg[Co(SCN)_4]$ as a calibrant. Mass spectra of the ligands were recorded on a LC/MS APCI AGILENT 1100 MSD spectrometer. $^1$H and $^{13}$C NMR spectra were recorded on a Bruker 400 MHz instrument. TMS was used as internal standard and $CDCl_3$ as solvent. The thermal analyses studies of the complexes were performed on a Perkin Elmer Pyris Diamond DTA/TG Thermal System under nitrogen atmosphere at a heating rate of 10 °C/min.

The microwave experiments were carried out in a Bergof MWS3+ (Germany) oven equipped with pressure and temperature control. Microwave experiments were done in closed DAP60 vessels. The reaction products were characterized and analyzed by using Perkin Elmer Clarus 600 GC (USA) equipped with MS detector fitted with Elite-5 MS and FID detector fitted with BPX5 capillary columns. A stock solution of concentration of $1 \times 10^{-4}$ M of Schiff base ligands was prepared in ethanol for electrochemical studies. All voltammetric measurements were performed using a BAS 100 W (Bioanalytical System, USA) electrochemical analyzer. A glassy carbon working electrode (BAS; $\Phi$: 3 mm diameter), an Ag/AgCl reference electrode (BAS; 3 M KCl) and platinum wire counter electrode and a standard one-compartment three electrode cell of 10 mL capacity were used in all experiments. The glassy carbon electrode was polished manually with aqueous slurry of alumina powder ($\Phi$: 0.01 μm) on a damp smooth polishing cloth (BAS velvet polishing pad), before each measurement. All measurements were performed at room temperature. A Mettler Toledo MP 220 pH meter was used for the pH measurements using a combined electrode (glass electrode reference electrode) with an accuracy of ±0.05 pH.

Data collection for X-ray crystallography was completed using a Bruker APEX2 CCD diffractometer and data reduction was performed using Bruker SAINT [18]. SHELXTL was used to solve and refine the structures [19].

### 2.2. Synthesis of the Schiff base ligands

The ligands were synthesized by the reaction of 6.3 mmol (1.0 g) naphthalene-1,5-diamine in 30 mL absolute methanol with 12.6 mmol (1.74 g) 2,3- and 2,4-dihydroxy benzaldehyde for $H_2L^1$ and $H_2L^2$, respectively, and with 12.6 mmol (1.92 g) o-vanillin for $H_2L^3$, each in 15 mL absolute methanol. The product was filtered, washed with cold solvent and recrystallized from a methanol/hexane mixture (1:1) to give colored crystals. Single crystals suitable for X-ray diffraction studies for $H_2L^1$ and $H_2L^3$ were obtained from slow evaporation of THF solution ligands. Physical properties and other spectroscopic data are given in the experimental section.

*$H_2L^1$:* ($C_{24}H_{18}N_2O_4$). Color: dark orange, yield: 85%, m.p.: 265 °C, elemental analyses: Found (calcd.), C, 72.41 (72.35); H, 4.49 (4.55); N, 6.98 (7.03). $^1$H NMR ($CDCl_3$, Δ (ppm)): 6.84–6.88 (m, 2H, aromatic H), 7.02–7.04 (m, 2H, aromatic H), 7.22–7.24 (m, 2H, aromatic H), 7.52–7.54 (m, 2H, aromatic H), 7.68–7.72 (m, 2H, aromatic H), 8.13–8.15 (m, 2H, aromatic H), 9.03 (s, 2H, CH═N), 9.38 (s, 2H, OH), 13.17 (s, 2H, OH). $^{13}$C NMR ($CDCl_3$, Δ (ppm)): 115.69 (aromatic C), 119.53–119.83 (aromatic C), 120.32 (aromatic C), 121.61 (aromatic C), 123.25 (aromatic C), 127.43 (aromatic C), 128.89 (aromatic C), 146.04–146.19 (Cq—OH), 149.76 (Cq—OH), 165.27 (C═N). FTIR (KBr, $cm^{-1}$): 3197 *ν*(OH), 1615 *ν*(C═N), 1350 *ν*(phenolic C—OH), 867 *ν*(aromatic ring C—H). Mass spectrum (LC/MS APCI): *m*/*z* 400 ($[M+2]^+$, 35%), 399 ($[M+1]^+$, 100%), 398 ($[M]^+$, 18%).

*$H_2L^2$:* ($C_{24}H_{18}N_2O_4$). Color: dark yellow, yield: 88%, m.p.: 276 °C. Elemental analyses: Found (calcd.), C, 72.30 (72.35); H, 4.59 (4.55); N, 7.08 (7.03). $^1$H NMR (CDCl3, Δ (ppm)): 10.37 (s, 2H, OH), 8.88 (s, 2H, OH), 8.81 (s, 2H, CH═N), 8.06–8.08 (m, 2H, aromatic H), 7.62–7.66 (m, 2H, aromatic H), 7.54–7.56 (m, 2H, aromatic H), 7.44–7.45 (m, 2H, aromatic H), 6.45–6.49 (m, 2H, aromatic H), 6.37–6.41 (m, 2H, aromatic H). $^{13}$C NMR (CDCl3, Δ (ppm)): 115.69 (aromatic C), 119.53–119.83 (aromatic C), 120.32 (aromatic C), 121.61 (aromatic C), 123.25 (aromatic C), 127.43 (aromatic C), 128.89 (aromatic C), 146.04–146-19 (Cq—OH), 149.76 (Cq—OH), 165.27 (C═N). FTIR (KBr, $cm^{-1}$): 3268 *ν*(OH), 2865 *ν*(C—H)alph, 1619 *ν*(C═N), 1300 *ν*(phenolic C—OH), 834 *ν*(aromatic ring, C—H). Mass spectrum (LC/MS APCI): *m*/*z* 399 ([M+1]+, 70%), 397 ([M−1]+, 20%), 325 ([M-$C_3H_5O_2$]+, 100%).

*$H_2L^3$:* ($C_{25}H_{22}N_2O_4$). Color: orange, yield: 83%, m.p.: 200 °C. Elemental analyses: Found (calcd.), C, 73.28 (73.23); H, 5.16 (5.20); N, 6.52 (6.57). $^1$H NMR ($CDCl_3$, Δ (ppm)): 3.87 (singlet, 3H, $OCH_3$), 6.95–6.99 (m, 3H, aromatic H), 7.19–7.21 (m, 2H, aromatic H), 7.36–7.38 (m, 2H, aromatic H), 7.52–7.54 (m, 2H, aromatic H), 7.76–7.70 (m, 3H, aromatic H), 8.12–8.14 (m, 2H, aromatic H), 9.05 (s, 2H, CH═N). $^{13}$C NMR ($CDCl_3$, Δ (ppm)): 56.45 ($OCH_3$), 115.69 (aromatic C), 116.37 (aromatic C), 119.36 (aromatic C), 120.21 (aromatic C), 121.74 (aromatic C), 124.23 (aromatic C), 127.42 (aromatic C), 128.88 (aromatic C), 146.13 (Cq—OH), 148.48 (Cq—OH), 150.93 ($OCH_3$), 165.27 (C═N). FTIR (KBr, $cm^{-1}$): 3201 *ν*(OH), 1605 *ν*(C═N), 1321 *ν*(phenolic C—OH), 838 *ν*(aromatic ring, C—H). Mass spectrum (LC/MS APCI): *m*/*z* 427 ($[M+1]^+$, 100%), 428 ($[M+2]^+$, 30%).

### 2.3. Preparation of the Schiff base complexes

The appropriate quantity of Schiff base ligands ($H_2L^1$, $H_2L^2$ and $H_2L^3$) (1 mmol) was dissolved in EtOH (20 mL). To this solution, a solution of the metal salts (1 mmol) in EtOH (20 mL) [1:2 M ratio (L:M)] was added. The mixture was stirred for 20 h at 80 °C. The precipitated complex was then filtered off, washed with cold ethanol and dried in a vacuum desiccator.

### 2.4. Cyclohexane and cyclooctane oxidation under microwave irradiation

The catalytic oxidation of cycloclohexane and cyclooctane under microwave irradiation was performed as follows: 0.02 mmol catalyst, 2 mmol cyclohexane (Carlo Erba, 99.8%), 4 mmol $H_2O_2$

**Table 1**
Crystallographic data of the Schiff base ligands $H_2L^1$ and $H_2L^3$.

| Identification code | $H_2L^1$ | $H_2L^3$ |
|---|---|---|
| Empirical formula | $C_{24}H_{18}N_2O_4$ | $C_{26}H_{22}N_2O_4$ |
| Formula weight | 398.40 | 426.46 |
| Crystal system | Triclinic | Monoclinic |
| Space group | $P\bar{1}$ | $P21/n$ |
| Unit cell | | |
| $a$ (Å) | 6.2762 (7) | 6.7449(5) |
| $b$ (Å) | 8.6491 (10) | 24.2256(17) |
| $c$ (Å) | 9.3158 (11) | 6.8765(5) |
| $\alpha$ (°) | 86.398 (2) | 90 |
| $\beta$ (°) | 82.908 (2) | 112.2940(10) |
| $\gamma$ (°) | 69.683 (1) | 90 |
| Volume (Å3) | 470.50 (9) | 1039.62(13) |
| $Z$ | 1 | 2 |
| Abs. coeff. ($mm^{-1}$) | 0.097 | 0.093 |
| Refl. collected | 5545 | 10504 |
| Ind. Refl. [$R_{int}$] | 1914 [0.0182] | 2575 [0.0166] |
| $R1$, $wR2$ [$I > 2\sigma$ ($I$)] | 0.0337, 0.0873 | 0.0374, 0.1018 |
| $R1$, $wR2$ (all data) | 0.0398, 0.0912 | 0.0418, 0.1056 |
| CCDC number | 847259 | 856306 |

**Table 2**
Hyrogen bond geometry.

| | D—H···A | D—H | H···A | D···A | <(DHA) |
|---|---|---|---|---|---|
| $H_2L^1$ | O1—H1···N1 | 0.95 | 1.73 | 2.5860(12) | 149.0 |
| $H_2L^3$ | O1—H1···N1 | 0.87 | 1.83 | 2.5987(12) | 145.9 |
| $H_2L^1$(inter-molecular) | O2—H2···O1# | 0.93 | 2.02 | 2.8333(12) | 145.4 |

Symmetry operation # $-x+1$, $-y+1$, $-z+1$.

(Merck, 35%) were microwaved for 60 min at 400 W (40% of maximum output power). The catalyst:substrate:oxidant ratio was 1:100:200. The complexes were dissolved in 5 mL acetonitrile and cyclohexane and $H_2O_2$ were added to the microwave vessels, for each oxidation experiment. After it was immediately closed the vessels, they were placed inside the Berghof MWS3+ microwave oven and irradiated at 400 W for 60 min. The temperature was controlled automatically by the microwave instrument at about 140 °C. However, for some short times, it increased to 150–160 °C during the reaction and consequently, the pressure also increased to 30–35 bar due to the evaporation of solvent and substrate. In order to stop the oxidation before analysis, 1 mL $H_2O$ was added in the vessels and the oxidized organic products, except organic acids, were extracted with 10 mL $CH_2Cl_2$ and injected to GC and GC–MS for analysis and characterization. The amounts of CyH, Cy—OH, Cy═O and CyON, CyON—OH, CyON═O present were calculated from external calibration curves that were prepared before analyses.

### 2.5. X-ray structure solution and refinement for the compounds

Data were collected at 150(2)K° on a Bruker ApexII CCD diffractometer using Mo-Kα radiation ($\lambda$ = 0.71073 Å). The structure was solved by direct methods and refined on $F^2$ using all the reflections [19]. All the non-hydrogen atoms were refined using anisotropic atomic displacement parameters and hydrogen atoms bonded to carbon atoms were inserted at calculated positions using a riding model. Hydrogen atoms bonded to phenolic oxygen atoms (O1 and O2) were located from difference maps and allowed to ride on their carrier atoms. Details of the crystal data and refinement are given in Table 1. Hydrogen bond parameters are listed in Table 2 and bond lengths and angles are given in Tables 3 and 4.

**Table 3**
Bond lengths [Å] and angles [°] for $H_2L^1$.

| | | | |
|---|---|---|---|
| C(1)—O(1) | 1.3598(14) | C(1)—C(2) | 1.3965(16) |
| C(1)—C(6) | 1.4065(17) | C(2)—O(2) | 1.3675(14) |
| C(2)—C(3) | 1.3828(17) | C(3)—C(4) | 1.3925(18) |
| C(4)—C(5) | 1.3796(18) | C(5)—C(6) | 1.4025(17) |
| C(6)—C(7) | 1.4514(16) | C(7)—N(1) | 1.2824(16) |
| N(1)—C(8) | 1.4190(15) | C(8)—C(9) | 1.3742(17) |
| C(8)—C(10) | 1.4263(17) | C(9)—C(12A) | 1.4079(17) |
| C(10)—C(11) | 1.4169(17) | C(10)—C(10A) | 1.424(2) |
| C(11)—C(12) | 1.3669(18) | C(12)—C(9A) | 1.4079(17) |
| O(1)—C(1)—C(2) | 117.92(10) | O(1)—C(1)—C(6) | 122.38(10) |
| C(2)—C(1)—C(6) | 119.71(11) | O(2)—C(2)—C(3) | 119.20(10) |
| O(2)—C(2)—C(1) | 120.78(10) | C(3)—C(2)—C(1) | 120.02(11) |
| C(2)—C(3)—C(4) | 120.54(11) | C(5)—C(4)—C(3) | 120.01(11) |
| C(4)—C(5)—C(6) | 120.39(12) | C(5)—C(6)—C(1) | 119.30(11) |
| C(5)—C(6)—C(7) | 120.40(11) | C(1)—C(6)—C(7) | 120.29(11) |
| N(1)—C(7)—C(6) | 121.84(11) | C(7)—N(1)—C(8) | 119.64(10) |
| C(9)—C(8)—N(1) | 121.25(11) | C(9)—C(8)—C(10) | 120.91(11) |
| N(1)—C(8)—C(10) | 117.78(10) | C(8)—C(9)—C(12A) | 120.28(11) |
| C(11)—C(10)—C(10A) | 119.54(14) | C(11)—C(10)—C(8) | 122.36(11) |
| C(10A)—C(10)—C(8) | 118.10(13) | C(12)—C(11)—C(10) | 120.67(11) |
| C(11)—C(12)—C(9A) | 120.50(11) | | |

Symmetry operations for equivalent atoms A $-x+1$, $-y$, $-z$.

**Table 4**
Bond lengths [Å] and angles [°] for $H_2L^3$.

| | | | |
|---|---|---|---|
| O(1)—C(1) | 1.3507(12) | C(1)—C(7) | 1.4068(14) |
| C(1)—C(2) | 1.4088(14) | C(2)—O(2) | 1.3612(13) |
| C(2)—C(4) | 1.3897(14) | O(2)—C(3) | 1.4296(13) |
| C(4)—C(5) | 1.4006(15) | C(5)—C(6) | 1.3763(15) |
| C(6)—C(7) | 1.4093(14) | C(7)—C(8) | 1.4535(14) |
| C(8)—N(1) | 1.2860(13) | N(1)—C(9) | 1.4145(12) |
| C(9)—C(10) | 1.3750(14) | C(9)—C(11) | 1.4298(14) |
| C(10)—C(13A) | 1.4083(15) | C(11)—C(12) | 1.4174(14) |
| C(11)—C(11A) | 1.4227(19) | C(12)—C(13) | 1.3692(15) |
| C(13)—C(10A) | 1.4084(15) | | |
| O(1)—C(1)—C(7) | 122.69(9) | O(1)—C(1)—C(2) | 117.71(9) |
| C(7)—C(1)—C(2) | 119.58(9) | O(2)—C(2)—C(4) | 125.65(9) |
| O(2)—C(2)—C(1) | 114.50(9) | C(4)—C(2)—C(1) | 119.83(9) |
| C(2)—O(2)—C(3) | 117.39(8) | C(2)—C(4)—C(5) | 120.26(9) |
| C(6)—C(5)—C(4) | 120.53(10) | C(5)—C(6)—C(7) | 120.10(10) |
| C(1)—C(7)—C(6) | 119.69(9) | C(1)—C(7)—C(8) | 120.56(9) |
| C(6)—C(7)—C(8) | 119.70(9) | N(1)—C(8)—C(7) | 121.60(9) |
| C(8)—N(1)—C(9) | 120.93(9) | C(10)—C(9)—N(1) | 122.17(9) |
| C(10)—C(9)—C(11) | 120.58(9) | N(1)—C(9)—C(11) | 117.18(9) |
| C(9)—C(10)—C(13A) | 119.99(10) | C(12)—C(11)—C(11A) | 119.27(11) |
| C(12)—C(11)—C(9) | 122.03(9) | C(11A)—C(11)—C(9) | 118.68(11) |
| C(13)—C(12)—C(11) | 120.40(9) | C(12)—C(13)—C(10A) | 121.06(10) |

Symmetry operations for equivalent atoms A $-x+2$, $-y$, $-z+2$.

## 3. Results and discussion

Analytical data for all of the complexes are given in Table 5 and are in good agreement with the expected values. To prepare the ligands $H_2L^1$, $H_2L^2$ and $H_2L^3$, we used the carbonyl and diamine compounds in ethanol media and the high yields suggest the reaction conditions were appropriate. The ligands have polar groups, such as —OH and —CH═N and are soluble in polar organic solvents, such as EtOH, MeOH and $CHCl_3$. The ligands are also stable for a long time at room temperature without decomposition to oxidized products. One difficulty in working with Schiff bases of salicylaldehyde derivatives arises from the fact that, even in neutral solutions, a number of species may be present. In addition to enolimines, hemiacetals and their hydrolysis products, tautomeric species, such as ketoamines or cyclicdiamines formed from mono-Schiff bases of diamines, may also occur. The metal complexes synthesized are also stable at room temperature and are soluble in polar organic solvents, such as EtOH, MeOH, DMSO and DMF.

**Table 5**
Analytical and physical data of the Schiff base ligands and their metal complexes.

| Compound | Color | Yield (%) | m.p. (°C) | % Found (Calcd.) | | |
|---|---|---|---|---|---|---|
| | | | | C | H | N |
| $Co_2(L^1)(H_2O)_2(Cl)_2$ | Brown | 66 | >250 | 46.45 (46.40) | 3.30 (3.25) | 4.54 (4.51) |
| $Cu_2(L^1)(H_2O)_2(Cl)_2$ | Brown | 72 | >250 | 46.97 (46.91) | 3.34 (3.28) | 4.61 (4.56) |
| $Cr_2(L^1)(H_2O)_4(NO_3)_4$ | Dark brown | 65 | >250 | 35.19 (35.13) | 3.02 (2.95) | 10.31 (10.24) |
| $Mn_2(L^1)(H_2O)_2(Cl)_2$ | Brown | 71 | >250 | 47.06 (47.01) | 3.35 (3.29) | 4.63 (4.57) |
| $Ru_2(L^1)(H_2O)_4(Cl)_4$ | Black | 68 | >250 | 35.54 (35.48) | 3.04 (2.98) | 3.50 (3.45) |
| $Co_2(L^2)(H_2O)_2(Cl)_2$ | Green | 70 | >250 | 46.45 (46.40) | 3.31 (3.25) | 4.55 (4.51) |
| $Cu_2(L^2)(H_2O)_2(Cl)_2$ | Black | 65 | >250 | 45.77 (45.72) | 3.25 (3.20) | 4.50 (4.44) |
| $Cr_2(L^2)(H_2O)_4(NO_3)_4$ | Brown | 60 | >250 | 35.18 (35.13) | 3.01 (2.95) | 10.30 (10.24) |
| $Mn_2(L^2)(H_2O)_2(Cl)_2$ | Brown | 68 | >250 | 47.06 (47.01) | 3.35 (3.29) | 4.62(4.57) |
| $Ru_2(L^2)(H_2O)_4(Cl)_4$ | Black | 67 | >250 | 35.54 (35.48) | 3.03 (2.98) | 3.51 (3.45) |
| $Co_2(L^3)(H_2O)_2(Cl)_2$ | Light brown | 70 | >250 | 48.15 (48.10) | 3.78 (3.73) | 4.36 (4.31) |
| $Cu_2(L^3)(H_2O)_2(Cl)_2$ | Black | 63 | >250 | 47.46 (47.42) | 3.72 (3.67) | 4.31 (4.25) |
| $Cr_2(L^3)(H_2O)_4(NO_3)_4$ | Brown | 65 | >250 | 36.86 (36.80) | 3.38 (3.33) | 9.95 (9.90) |
| $Mn_2(L^3)(H_2O)_2(Cl)_2$ | Brown | 69 | >250 | 48.75 (48.70) | 3.82 (3.77) | 4.43 (4.37) |
| $Ru_2(L^3)(H_2O)_4(Cl)_4$ | Black | 65 | >250 | 37.21 (37.16) | 3.40 (3.36) | 3.38 (3.33) |

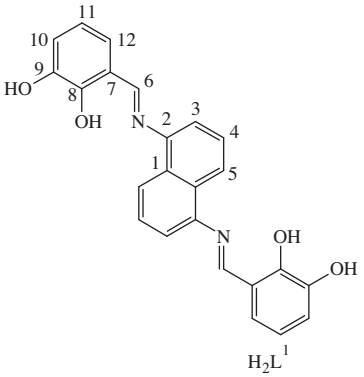


$H_2L^1$

$C_1$ : 164.04 $C_8$ : 149.76 $H_3$: 7.54
$C_2$ : 128.94 $C_9$ : 146.19 $H_4$: 7.68
$C_3$ : 115.68 $C_{10}$ : 119.83 $H_5$: 8.14
$C_4$ : 127.43 $C_{11}$ : 119.53 $H_{10}$: 6.86
$C_5$ : 121.61 $C_{12}$ : 123.25 $H_{11}$: 7.02
$C_6$ : 165.27 $H_{12}$: 7.22
$C_7$ : 120.32

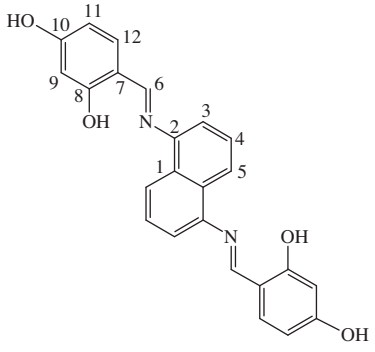


$H_2L^2$

$C_1$ : 163.26 $C_8$ : 146.30 $H_3$: 7.44
$C_2$ : 128.98 $C_9$ : 102.88 $H_4$: 7.63
$C_3$ : 115.30 $C_{10}$ : 163.99 $H_5$: 8.65
$C_4$ : 127.23 $C_{11}$ : 108.57 $H_9$: 6.39
$C_5$ : 121.05 $C_{12}$ : 135.01 $H_{11}$: 6.47
$C_6$ : 163.42 $H_{12}$: 7.54
$C_7$ : 115.30

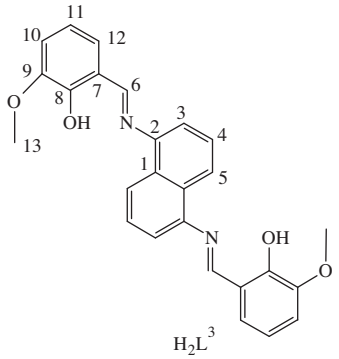


$H_2L^3$

$C_1$ : 146.13 $C_8$ : 150.93 $H_3$ : 7.44
$C_2$ : 128.88 $C_9$ : 148.48 $H_4$ : 7.68
$C_3$ : 115.69 $C_{10}$ : 119.36 $H_5$ : 8.13
$C_4$ : 127.42 $C_{11}$ : 116.37 $H_{10}$ : 6.97
$C_5$ : 121.74 $C_{12}$ : 124.23 $H_{11}$ : 7.20
$C_6$ : 164.86 $C_{13}$ : 56.45 $H_{12}$ : 7.37
$C_7$ : 120.21 $H_{13}$ : 3.87

**Fig. 1.** $H^1(^{13}C)$ NMR data of the Schiff base ligands.

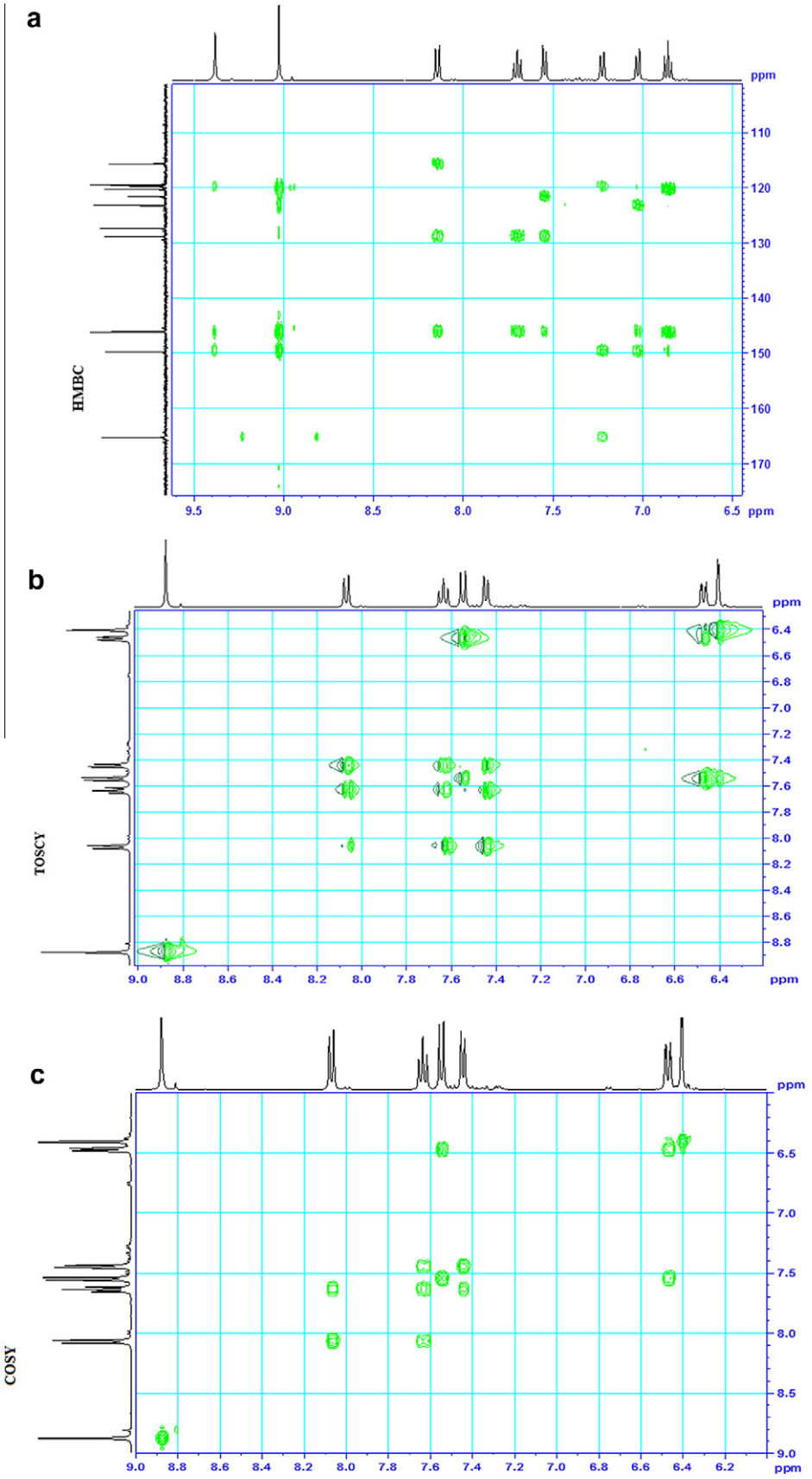


**Fig. 2.** The HMBC (a: $H_2L^1$), TOCSY (b: $H_2L^2$) and COSY (c: $H_2L^2$) spectra of the Schiff base ligands $H_2L^1$ and $H_2L^2$.

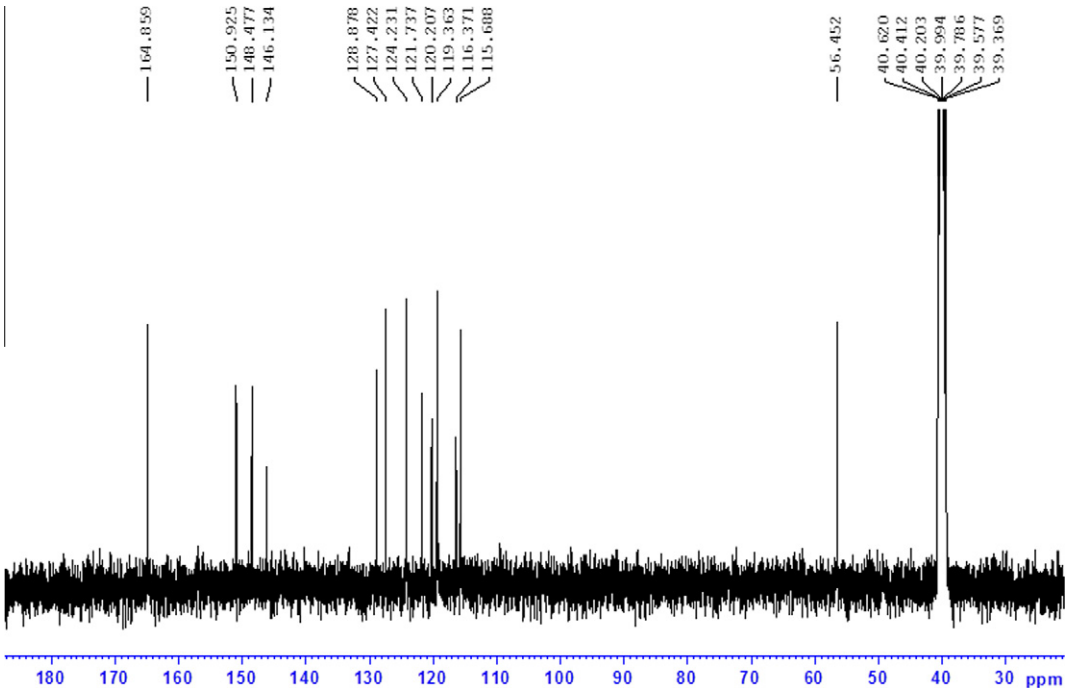


**Fig. 3.** The $^{13}C$ NMR spectrum of the Schiff base ligand $H_2L^3$.

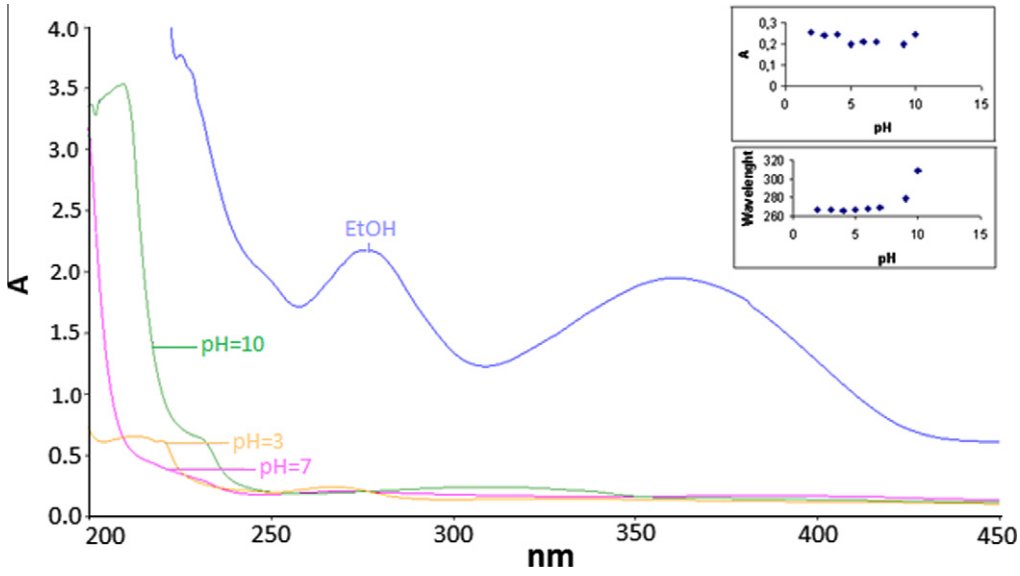


**Fig. 4.** The absorption spectra of the ligand $H_2L^1$ ($1 \times 10^{-4}$ M) in the different pH values.

The $^1H$ and $^{13}C$ NMR spectra of the ligands were recorded in $CDCl_3$ and data are given in the experimental section. All $^1H$ and $^{13}C$ NMR signals were completely assigned using $^1H$–1H COSY, HETCOR, TOSCY and HMBC spectra. The ring carbon atoms of the ligands were elucidated by the interpretation of $^{13}C$ 1H COSY, $^1H$–1H COSY, HETCOR and HMBC experiments and assignments are given in Fig. 1. The HMBC spectrum of the ligand $H_2L^1$ and TOSCY and COSY spectra of the ligand $H_2L^2$ are shown in Fig. 2. It is noteworthy that the influence of substitution on the chemical shifts of the naphthalene moiety is weak. The OH groups on the salicylidene moiety increases the electron density of the aromatic rings due to the resonance or mesomeric effect. The Schiff base ligands have the proton donor OH groups in the *ortho* position of their aromatic rings. Due to the presence of OH groups in the *ortho* position to imine group, formation of intramolecular hydrogen bonds is possible. The $^1H$ resonance of the O—H groups of the ligands was shown in the 10.37–13.50 ppm range. The signal due to the OH proton disappears on $D_2O$ shake. The singlets in the 8.87–9.38 ppm range can be attributed to the protons of the azomethine groups.

The COSY spectrum of the ligand $H_2L^1$ shows the protons $H_3$, $H_4$ and $H_5$ are vicinal. The proton $H_4$ interacts with both $H_3$ and $H_5$. The proton $H_4$ is shown at 7.68 ppm as a triplet. However, the protons $H_3$ and $H_5$ are doublets at 7.54 and 8.14 ppm, respectively. The proton $H_{11}$ interacts with $H_{10}$ and $H_{12}$. Therefore, the proton $H_{11}$ appears as a triplet at 6.86 ppm, while $H_{10}$ and $H_{12}$ appear as doublets at 7.02 and 7.23 ppm. Using the HETCOR spectrum of $H_2L^1$, the carbon atoms $C_3$ ($\Delta$: 115.68), $C_4$ ($\Delta$: 127.43), $C_5$ ($\Delta$: 121.61),

$C_{10}$ (Δ: 119.83), $C_{11}$ (Δ: 119.53) and $C_{12}$ (Δ: 123.25) were assigned. In the spectra of the other ligands $H_2L^2$ and $H_2L^3$, similar correlations and interactions were determined. From the HMBC spectrum of the ligand $H_2L^1$, the azomethine carbon atoms were investigated at 165.27 ppm as $C_6$. In the other ligands, this carbon atom was seen at 163.42 and 164.86 ppm. In the spectrum of the ligand $H_2L^3$, the methoxy carbon atom was identified at 56.45 ppm as $C_{13}$. The $^{13}C$ NMR spectrum of the Schiff base ligand $H_2L^3$ is given in Fig. 3. The mass spectral data of the ligands are given in the experimental section. The formulation of the ligands are deduced from analytical data, $^1H(^{13}C)$ NMR and further supported by mass spectroscopy. The relatively low intensities of the molecular ion peaks, $[M]^+$, are indicative of the ease of fragmentation of the compounds, and this may reflect the number of heteroatoms present in each structure. The spectra of the ligands $H_2L^1$ and $H_2L^2$ show $[M+1]^+$, peaks at $m/e$ 399 while for $H_2L^3$ the signal is at $m/e$ = 427. The mass spectra of the investigated compounds are relatively complicated and exhibit a large number of peaks. Nevertheless, all of the spectra are very similar, indicating the close structural resemblance of the compounds. The fragmentation mode, considered most likely to be the same for all of the complexes, follow common steps. The mass spectra of all the complexes exhibit the presence of molecular ion peaks of weak intensity, dication $[M_2(L^n)](H_2O)_2(Cl)_2]^{2+}$.

Electronic spectra of the ligands ($H_2L^1$, $H_2L^2$ and $H_2L^3$) were investigated at $1 \times 10^{-3}$ M in ethanol solution and at different pH values (pH 2–12) in phosphate buffer. The spectra are pH dependent because of the weak acid character of the ligands. If all ligands having $H_2L^n$ ($n$: 1, 2 or 3) are shown as $H_2A$, in solution; the equilibrium is:

$$H_2A \leftrightarrow 2H^+ + A^{2-}$$

If we take the negative logarithm of the equilibrium constant, we get $pK_a = pH + \log [H_2A]/[A^{2-}]$. When $[H_2A] = [A^{2-}]$, then p$K$a has to equal pH and this point is also named the half titration pH point, because at this point, the half of the $[H_2A]$ concentration is titrated. Using these equations, $K_a$ values of all three species can be obtained. To calculate the p$K$a values, the variation of absorption with pH was investigated. The absorption spectra of the ligand $H_2L^1$ in the $1 \times 10^{-4}$ M concentration are shown in Fig. 4. The ligand $H_2L^1$ has two absorption maxima in the 270–400 nm range. It shows $\pi \rightarrow \pi^*$ transition at 276 and $n \rightarrow \pi^*$ at 381 nm. The absorption maxima at 381 nm was shifted to shorter absorption values in the pH 2–12 range. In the pH 2–12 range, the ligand shows a hypsochromic shift in this solution. As the pH values increase, the wavelength shifted to the longer regions. In this pH range, there is also a bathochromic shift. Similar data were also obtained for the ligands $H_2L^2$ and $H_2L^3$ in ethanol solution.

Electronic spectra of the metal complexes were measured in EtOH and the numerical data are given in Table 6. All the complexes show an intense band in the 330–300 nm range which is assigned to a $\pi$–$\pi^*$ transition associated with the azomethine linkage [20]. The spectra of the complexes show intense bands in the high-energy region in the 480–340 nm range which can be assigned to charge transfer L → M bands [21]. The bands observed in the 740–510 nm region can be attributed to $d$–$d$ transitions of the metal ions. In the spectra of the Cu(II) complexes, the $d$–$d$ transitions are observed in the 730–510 nm range. These values are of particular importance since they are highly dependent on the geometry of the molecule. It is known that the transitions from a square-planar structure to a deformed tetrahedral structure lead to a red shift of absorption in the electronic spectra [22]. Thus, the smaller value of the wavelength of the band corresponding to the transitions is resemblance between the geometry of the complex and that of square–planar complex.

IR data of the complexes are given in Table 6. In the spectra (in the experimental section) of the Schiff base ligands $H_2L^1$, $H_2L^2$ and $H_2L^3$, the broad bands in the 3268–3197 $cm^{-1}$ range can be attributed to the $\nu$(OH) $cm^{-1}$ vibration. In the transition metal complexes, the bands due to the OH modes are no longer observed, suggesting that all the hydroxyl protons are displaced by $M^{II}$ and $M^{III}$ ions leading to covalent $\nu$(M—O) bonding with the ligands. In the ligands, the broad bands at 2750 and 2585 $cm^{-1}$ come from intramolecular hydrogen bonding along the phenolic –OH and azomethine —CH=N— groups, these bands disappear on complexation between the oxygen and nitrogen atoms with metal ions. The $\nu$(CH=N) band (1619–1605 $cm^{-1}$) is shifted to lower wavenumbers denoting that the nitrogen atom of the azomethine group is coordinated to the metal(II) ion. The bonding of the metal ions to the ligands through the nitrogen and oxygen atoms is further supported by the presence of new bands in the 565–470 and 475–430 $cm^{-1}$ range due to the $\nu$(M—O) and $\nu$(M—N) vibrations, respectively.

In order to investigate the metal–halogen, metal–nitrogen and metal–oxygen vibrations, the far infrared spectra of the complexes were studied and data for metal complexes of ligand $H_2L^1$ are given in Fig. 5. The far infrared spectra of the chloro complexes revealed some new bands in the 318–307, 294–293, 280–276 and 272–270 $cm^{-1}$ range, which are assigned to $\nu$(Co—Cl), $\nu$(Ru—Cl), $\nu$(Mn—Cl) and $\nu$(Cu—Cl), respectively. The presence of bands in the 475–430 $cm^{-1}$ range in the complexes originates from the $\nu$(M—N) (azomethine) vibration and substantiates this coordination. In the Cr(III) complexes, the coordination of nitrate groups

**Table 6**
Magnetic, infrared[a] and electronic spectral data of the metal complexes.

| Compound | $\nu$ (OH) | $\nu$ (CH=N) | $\nu$ (C—OH) | $\nu$ (M—N) | $\nu$ (M—O) | $\nu$ (M—Cl) | $\nu$ (Cr—$ONO_2$) | $\lambda_{max}$ (nm, MeOH) | $M_{eff}$ (B.M.) |
|---|---|---|---|---|---|---|---|---|---|
| $Co_2(L^1)(H_2O)_2(Cl)_2$ | 3218 | 1604 | 1315 | 494 | 462 | 312 | | 675, 610, 375, 360, 310, 290, 285 | 4.22 |
| $Cu_2(L^1)(H_2O)_2(Cl)_2$ | 3250 | 1621 | 1322 | 500 | 475 | 316 | | 730, 405, 350, 320, 285 | 1.82 |
| $Cr_2(L^1)(H_2O)_4(NO_3)_4$ | 3212 | 1605 | 1321 | 482 | 460 | | 243 | 440, 390, 325, 280 | 3.6 |
| $Mn_2(L^1)(H_2O)_2(Cl)_2$ | 3285 | 1603 | 1345 | 470 | 474 | 278 | | 735, 380, 305,290, 265 | 5.88 |
| $Ru_2(L^1)(H_2O)_4(Cl)_4$ | 3224 | 1612 | 1305 | 490 | 467 | 294 | | 590, 355, 320, 295, 270 | 1.81 |
| $Co_2(L^2)(H_2O)_2(Cl)_2$ | 3268 | 1607 | 1318 | 489 | 462 | 310 | | 680, 600, 390, 380, 320, 278 | 4.26 |
| $Cu_2(L^2)(H_2O)_2(Cl)_2$ | 3275 | 1617 | 1322 | 470 | 484 | 272 | | 620, 380, 320, 295, 280 | 1.90 |
| $Cr_2(L^2)(H_2O)_4(NO_3)_4$ | 3206 | 1603 | 1315 | 490 | 460 | | 240 | 480, 410, 375, 320, 280 | 3.8 |
| $Mn_2(L^2)(H_2O)_2(Cl)_2$ | 3308 | 1606 | 1349 | 474 | 470 | 280 | | 738, 390, 325, 280 | 5.90 |
| $Ru_2(L^2)(H_2O)_4(Cl)_4$ | 3288 | 1609 | 1350 | 480 | 475 | 293 | | 580, 400, 375, 330, 290, 280, 275 | 1.83 |
| $Co_2(L^3)(H_2O)_2(Cl)_2$ | 3305 | 1613 | 1310 | 492 | 465 | 309 | | 670, 610, 460, 380, 330, 280 | 4.24 |
| $Cu_2(L^3)(H_2O)_2(Cl)_2$ | 3280 | 1603 | 1305 | 464 | 472 | 271 | | 510, 475, 340, 307, 280 | 1.88 |
| $Cr_2(L^3)(H_2O)_4(NO_3)_4$ | 3278 | 1600 | 1318 | 480 | 470 | | 235 | 400, 390, 300, 280 | 3.8 |
| $Mn_2(L^3)(H_2O)_2(Cl)_2$ | 3374 | 1603 | 1325 | 488 | 467 | 284 | | 740, 380, 325, 275 | 5.90 |
| $Ru_2(L^3)(H_2O)_4(Cl)_4$ | 3265 | 1605 | 1349 | 465 | 475 | 294 | | 600, 450, 340, 315, 290 | 1.82 |

[a] $cm^{-1}$.

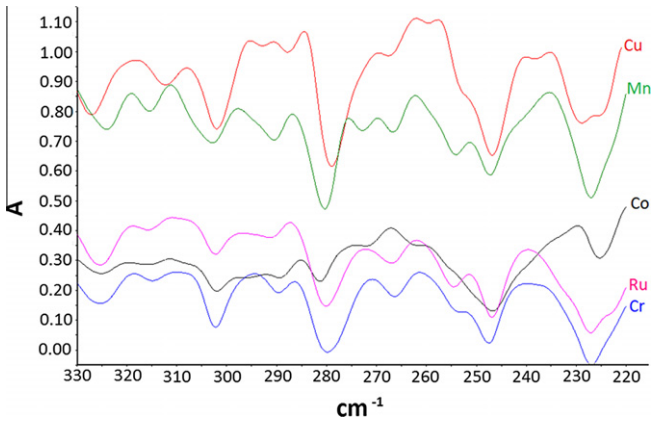


**Fig. 5.** The Far-IR spectra of the transition metal complexes of the Schiff base ligand $H_2L^1$.

is further supported by the appearance of new bands in the 245–230 $cm^{-1}$ range.

The molar conductivities (see Table 6) in DMF ($\sim 10^{-3}$ M solutions) are too low to account for any dissociation of the Schiff base ligands and complexes in MeOH. Therefore, the all compounds can be regarded as non-electrolytes [23].

The magnetic moments (as B.M.) of the complexes were measured at room temperature and data are given in Table 6. All cobalt(II) complexes of the ligands $H_2L^1$–$H_3L^2$ have magnetic moments values in the 4.23–4.26 B.M. range, and these values are consistent with tetrahedral geometry [24]. The proposed structures of the binuclear Cu(II) complexes are supported by magnetic moment data. The observed magnetic moment values of the binuclear Cu(II) complexes of the ligands $H_2L^1$–$H_2L^3$ are in the 1.82–1.90 B.M. We can suggest that the binuclear Cu(II) complexes have tetrahedral structure around the central metal ions. We may anticipate that in Cr(III), however, the unpaired spins are in $t_{2g}$ orbitals (for octahedral coordination). Schiff base Cr(III) complexes exhibited magnetic moments in the range 3.6–3.8 B.M., consistent with $S = 3/2$ spin states of Cr(III) $d^3$ centers. The Mn(II) Schiff base complexes show the absorption bands in the 740–735 nm range and these data are consistent with a four-coordinate, tetrahedral geometry [25]. At room temperature, the magnetic moment data of the complexes are in the 5.88–5.90 B.M range and these data are usually observed for the Mn(II) compounds, regardless of stereochemistry because the ground term is an $^6A_1$, and thus, orbital contribution is nil. The Mn(II) complexes have the tetrahedral geometry [26]. The effective magnetic moments of the Ru(III) complexes are in the 1.81–183 B.M. at room temperature, a little higher than expected for the spin-only value of a single-unpaired electron (1.73 B.M.), which is consistent with a paramagnetic low-spin Ru(III) [27].

### 3.1 Crystal structures of the Schiff base ligand $H_2L^1$and $H_2L^3$

Perspective views of $H_2L^1$ and $H_2L^3$ are shown in Fig. 6. All bond lengths and angles are within the normal ranges. All bond lengths and angles in the phenyl rings and naphthalene ring have normal *Csp2–Csp2* values. The azomethine linkage distances in $H_2L^1$ and $H_2L^3$ are 1.2824(16) and 1.2860(13) Å, respectively, which are within the range of normal C=N values. Both $H_2L^1$ and $H_2L^3$ are centrosymmetric. The molecular structures are broadly similar. The dihedral angle between the two identical aromatic rings and naphthalene ring in $H_2L^1$ and $H_2L^3$ are 56.40(6) and 47.03(7)°, respectively; this difference is possibly due to an additional intermolecular hydrogen bond in $H_2L^1$.

There are intramolecular phenol-imine hydrogen bonds in both $H_2L^1$ and $H_2L^3$ between O1—N1 (Table 2). Compound $H_2L^1$ contains a second phenol group and this makes an intermolecular hydrogen bond with the phenolic oxygen atom of a neighboring molecule O2—O1 (under symmetry operation $-x+1, -y+1, -z+1$), linking the molecules into H-bonded chains (Figs. 8 and 9).

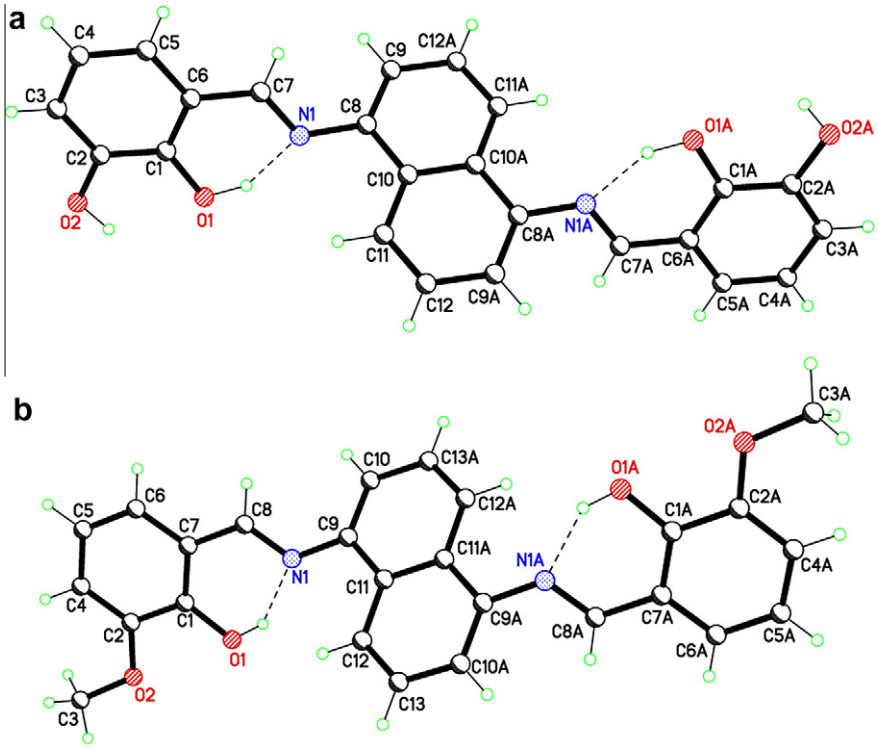


**Fig. 6.** Perspective view of $H_2L^1$ (a) and $H_2L^3$ (b) with atom labeling, thermal ellipsoid 50% probability, intramolecular hydrogen bonds are shown as dash lines, symmetry operations: $H_2L^1$ A; $-x+1, -y, -z$ $H_2L^3$ A; $-x+2, -y, -z+2$.

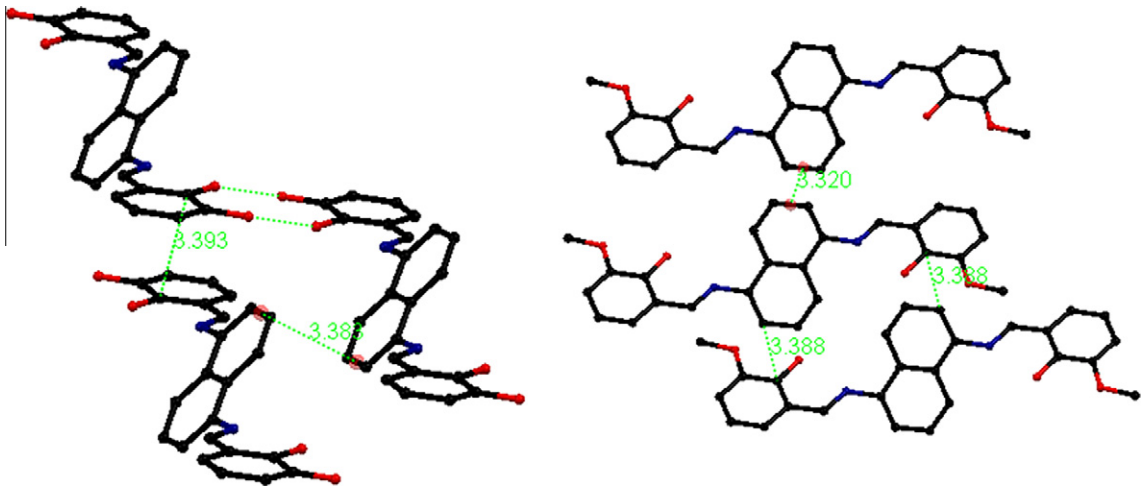


**Fig. 7.** Molecular interactions within the structures ($H_2L^1$ left, $H_2L^3$ right).

In $H_2L^1$, intermolecular hydrogen linked chains link with neighboring chain via π–π edge to edge interactions; there are two sets of interactions with neighboring molecules. First, one edge of the naphthalene ring (C9 and C12) is stacked with the same section of an adjacent molecule (under symmetry operation $1 + x, y, z$) with a interplanar separation of 3.383 Å. Second, phenol-imine section (N1—C2) is stacked with the same section of an adjacent molecule (under symmetry operation $-x, 1 - y, 1 - z$); C1 and C1 are separated by 3.393 Å (Fig. 7).

Similar π–π edge to edge interactions were observed in $H_2L^3$. The C10—C13 edge of the naphthalene ring is stacked with the same section of an adjacent molecule (under symmetry operation $1 + x, y, z$) with a interplanar separation of 3.320 Å. Additionally, there are also π–π edge to face (naphthalene–phenol) interactions in $H_2L^3$; C10 is stacked with C1 of the neighboring molecule (under symmetry operation $x, y, -1 + z$) with a separation of 3.388 Å (Fig. 10). Unit cell packing is determined by intermolecular hydrogen bonds and π–π interactions in $H_2L^1$ and π–π interactions in $H_2L^3$ (Figs. 8 and 9).

### 3.2. Electrochemical studies

Cyclic voltammograms of the complexes were run in DMF-0.1 M $Bu_4NBF_4$ as supporting electrolyte at 293 K. All potentials quoted refer to measurements run at a scan rates in the 100–500 $mVs^{-1}$ range and against an internal ferrocene–ferrocenium standard, unless otherwise stated. The electrochemical studies were done in the $1 \times 10^{-3}$ and $1 \times 10^{-4}$ M solutions and obtained data are given in Table 7. The voltammograms were recorded in the range from −2.0 to 2.0 V vs Ag/AgCl. The selective voltammograms of the complexes $Co_2(L^1)(H_2O)_2(Cl)_2$ (a), $Cu_2(L^1)(H_2O)_2(Cl)_2$ (b), $Mn_2(L^2)(H_2O)_2(Cl)_2$ (c) and $Cu_2(L^3)(H_2O)_2(Cl)_2$ (d) are shown in Fig. 6a–d. The complex $Co_2(L^1)(H_2O)_2(Cl)_2$ (Fig. 11a) shows irreversible two anodic potentials at about 1.08 and 1.54 V. The sharp oxidation peak at about 1.54 V is assigned to the oxidation of the Co(II) complex. The sharpness of oxidation peak of cobalt is due to the stability of Cu(II) in the solution. During the reverse scan, a poorly defined oxidation wave appears at −0.68 V, which is associated with the cathodic peak. The sharp oxidation peak assigned to cobalt is also seen in a separate CV scan ranging from 1.20 to 0 V but not in a scan from 0 to 1.20 V (not shown). Thus, it is concluded that the complex is decomposed. Other Co(II) complexes also display similar properties.

The complex $Cu_2(L^1)(H_2O)_2(Cl)_2$ (Fig. 11b) shows one irreversible reduction wave ($\Delta E = 40$ mV) on the negative side against $Ag^+$/AgCl, and one irreversible oxidation wave ($\Delta E = 90$ mV) on the positive side. The redox process is assigned to $Cu^{2+}/Cu^{3+}$ oxidation. In the reverse scan, $Cu^{2+}/Cu^{1+}$ was observed in the cathode sweep. On the other hand, the $Cu_2(L^2)(H_2O)_2(Cl)_2$ and $Cu_2(L^3)(H_2O)_2(Cl)_2$ complexes have two irreversible oxidation and

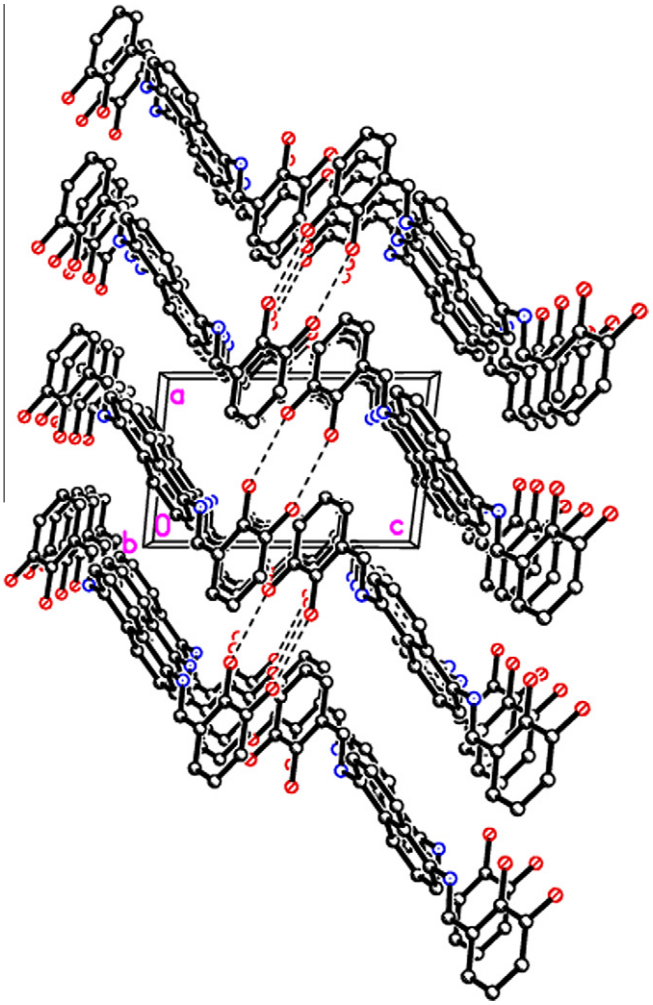


**Fig. 8.** Packing plot of $H_2L^1$ viewing down b axis, hydrogen atoms are omitted for clarity, intermolecular, and hydrogen bonds are shown as dash lines.

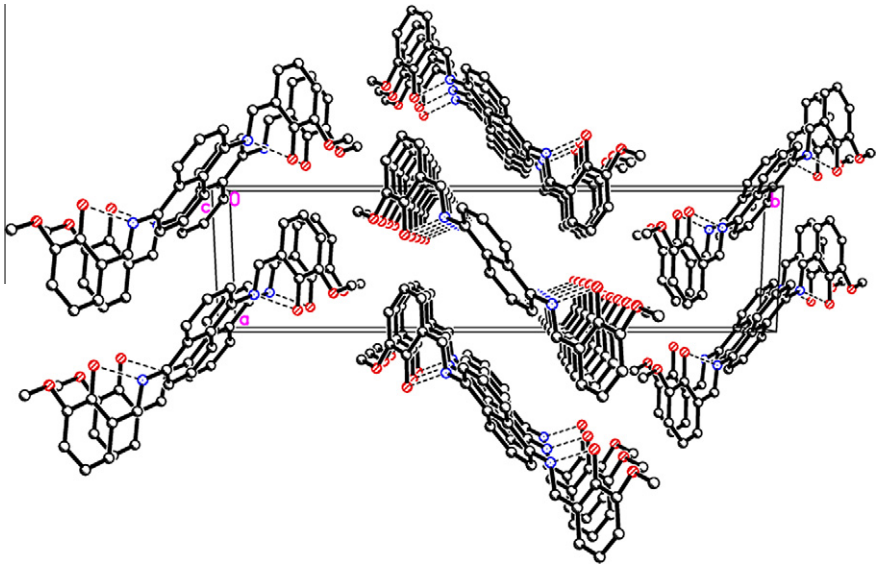

**Fig. 9.** Packing plot of $H_2L^3$ viewing down c axis, hydrogen atoms are omitted for clarity, intramolecular, and hydrogen bonds are shown as dash lines.

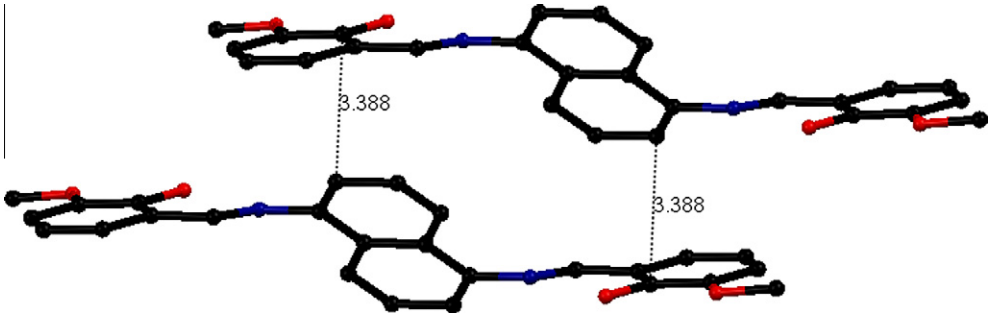


**Fig. 10.** Face to edge interactions within the structure of the ligand $H_2L^3$.

reduction waves in the 1.55–0.70 V range and −0.35 to 1.1 V range. The irreversibility of the redox processes in the complexes is attributed to the changes in the coordination geometry or coordination number upon change of the oxidation state or even to the expulsion of metal ions from the coordination sphere.

Fig. 11c shows the cyclic voltammogram of $Mn_2(L^2)(H_2O)_2(Cl)_2$. Cyclic voltammetry studies provide additional useful information about the structure of these compounds. The complexes exhibit two/three reduction–oxidation waves (see Table 7) in the range −1.42 to 1.59 V ($E_{pa}$) and −0.89 to 1.37 V ($E_{pc}$), which suffer an irreversible one-electron oxidation process $[Mn^{II}] \rightarrow [Mn^{III}] + e^-$. The $Mn_2(L^2)(H_2O)_2(Cl)_2$ complex has reversible reduction–oxidation process at about 1.40 V. This complex exhibits higher current intensities in its redox waves than other Mn(II) complexes. These

**Table 7**
The electrochemical data of the Schiff base transition metal complexes.

| Compound | $E_{pa}$(V) (i)/(ii) | $E_{pc}$(V) (i)/(ii) | $E_{1/2}$(V) (i)/(ii) | $\Delta E_p$(V) (i)/(ii) |
|---|---|---|---|---|
| $Co_2(L^1)(H_2O)_2(Cl)_2$ | 1.08, 1.54 (1.11, 1.58) | 0.69, −0.68 (0.65, −0.71) | – | 0.39 (0.46) |
| $Cu_2(L^1)(H_2O)_2(Cl)_2$ | 0.87 (0.91) | 0.69 (0.78)) | – | 0.18 (0.22) |
| $Cr_2(L^1)(H_2O)_4(NO_3)_4$ | −1.61, 0.97 (−1.58, −1.08, 0.24) | 0.91, 1.11 (1.12, −0.88, −1.72) | 0.94 (–) | 0.08 (0.64) |
| $Mn_2(L^1)(H_2O)_2(Cl)_2$ | 0.88, 1.31 (0.83, 1.40) | 0.69, 0.37 (1.37, 0.60, 0.33) | – (1.38) | 0.19 (0.03) |
| $Ru_2(L^1)(H_2O)_4(Cl)_4$ | 1.07, 1.58 (0.36, 1.13) | 0.81, 0.32, (0.85, 0.28) | – | 0.26 (0.08) |
| $Co_2(L^2)(H_2O)_2(Cl)_2$ | −0.33, 1.59 (−0.27, 1.02) | 1.15, −0.89 (1.09, −0.92) | – (1.06) | 0.44 (0.65) |
| $Cu_2(L^2)(H_2O)_2(Cl)_2$ | 0.20, 0.95 (0.18, 0.93) | 0.70 (0.68) | – (1.12) | 0.23 (0.54) |
| $Cr_2(L^2)(H_2O)_4(NO_3)_4$ | −0.35, 1.01 (−0.32, 1.11) | 1.20, −0.76 (1.22, −0.83) | – (1.16) | 0.41 (0.51) |
| $Mn_2(L^2)(H_2O)_2(Cl)_2$ | 0.98, 1.53 (−0.32, 1.04, 1.59) | 1.16, −0.79 (1.04, −0.86) | – (1.04) | 0.43 (0.55) |
| $Ru_2(L^2)(H_2O)_4(Cl)_4$ | 0.71, 1.54 (0.22, 1.65) | 0.95, −0.88 (0.97, −0.93) | – | 0.16 (0.11) |
| $Co_2(L^3)(H_2O)_2(Cl)_2$ | −1.21, 1.67 (−1.45, 1.51) | 1.06, −1.06 (1.00, −0.82) | – | 0.61 (0.51) |
| $Cu_2(L^3)(H_2O)_2(Cl)_2$ | 0.21, 1.05 (0.24, 1.14) | 1.26, 0.53 (1.24, 0.50) | – | 0.34 (0.45) |
| $Cr_2(L^3)(H_2O)_4(NO_3)_4$ | 0.89 (0.92) | 1.14, 0.71 (1.19, 0.68) | – | 0.78 (0.14) |
| $Mn_2(L^3)(H_2O)_2(Cl)_2$ | −1.42, −0.37, 1.46 (−1.31, 1.58) | 1.06, −0.82 (1.03, −0.89) | – | 0.45 (0.55) |
| $Ru_2(L^3)(H_2O)_4(Cl)_4$ | −1.50, 0.72 (−1.44, 0.35) | 0.97, −1.46 (0.96, −1.00) | −1.48 (–) | 0.25 (0.69) |

Supporting electrolyte: $[NBu_4](BF_4)$ (0.1 M); concentrations of the compounds: $1 \times 10^{-3}$ M. All the potentials are referenced to $Ag^+$/AgCl; where $E_{pa}$ and $E_{pc}$ are anodic and cathodic potentials, respectively. $E_{1/2} = 0.5 \times (E_{pa} + E_{pc})$, $\Delta E_p = E_{pa} - E_{pc}$. (i): these data have been obtained from scan rate 250 $mVs^{-1}$. Other data (ii) have been obtained by scan rate 500 $mVs^{-1}$.

complexes, that incorporate Schiff bases with electron donor substituents in the phenyl rings, show a greater tendency to stabilize manganese (III).

The cyclic voltammograms of the Schiff base Cr(III) complexes show two irreversible one-electron oxidation waves in the −1.61 to 1.11 V range. There are no redox waves observed for the free Schiff base ligands, strongly suggesting that these potentials are due to oxidation from Cr(III) to Cr(IV). The high oxidation potential indicates that the Cr(III) oxidation state in $Mn_2(L^3)(H_2O)_4(NO_3)_4$ is highly stabilized and it is difficult to oxidize the Cr(III) to Cr(IV) in the other Cr(III) complexes. The $Mn_2(L^2)(H_2O)_4(NO_3)_4$ complex has a reversible process at about 1.11 V. Comparison of cyclic voltammograms of the Cr(III) complexes and the ligands indicate that both redox waves involve only the metal center. We also examined

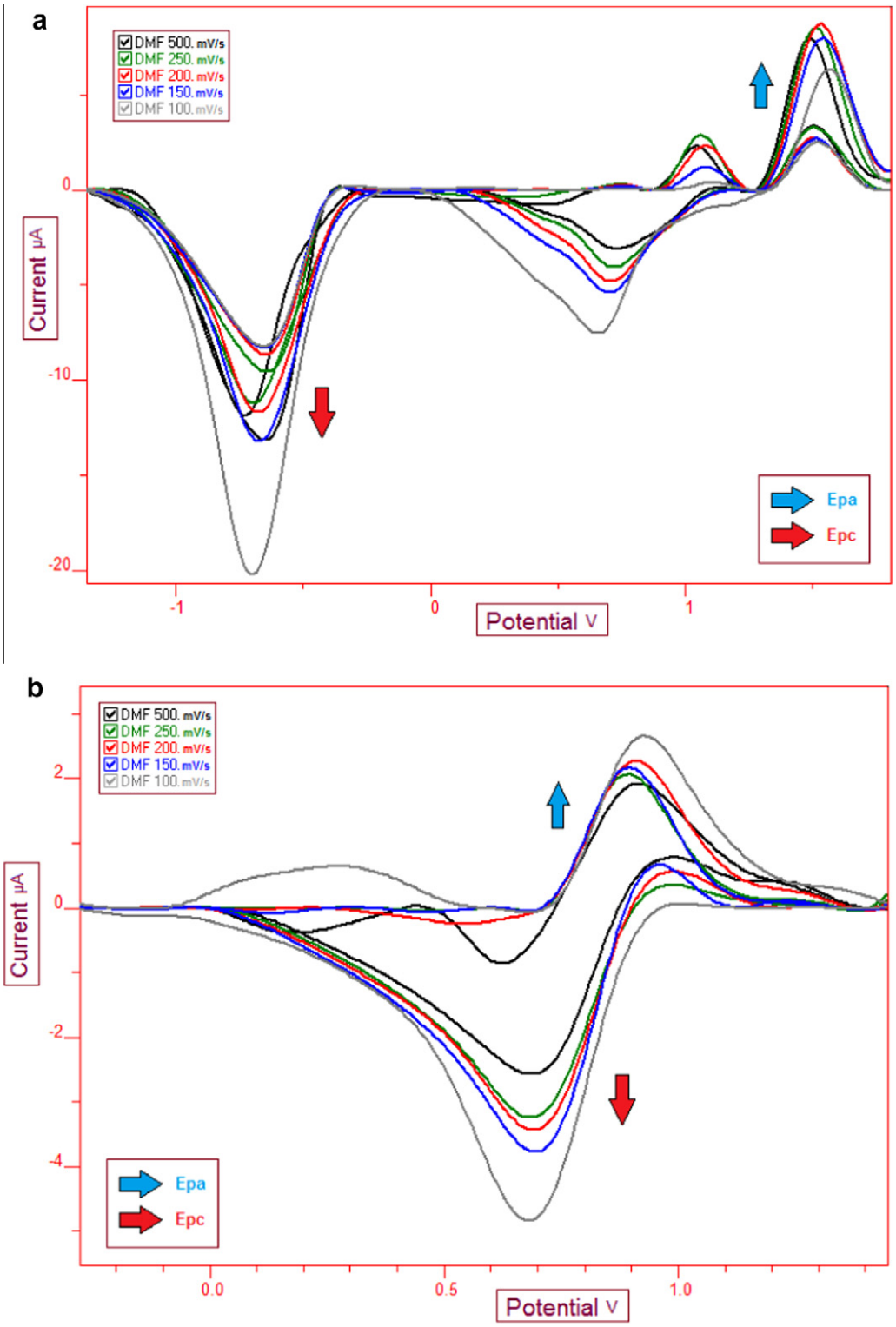


**Fig. 11.** (a–d) Cyclic voltammograms of the $Co_2(L^1)(H_2O)_2(Cl)_2$ (a), $Cu_2(L^1)(H_2O)_2(Cl)_2$ (b), $Mn_2(L^2)(H_2O)_2(Cl)_2$ (c) and $Cu_2(L^3)(H_2O)_2(Cl)_2$ (d) complexes at the different scan rates.

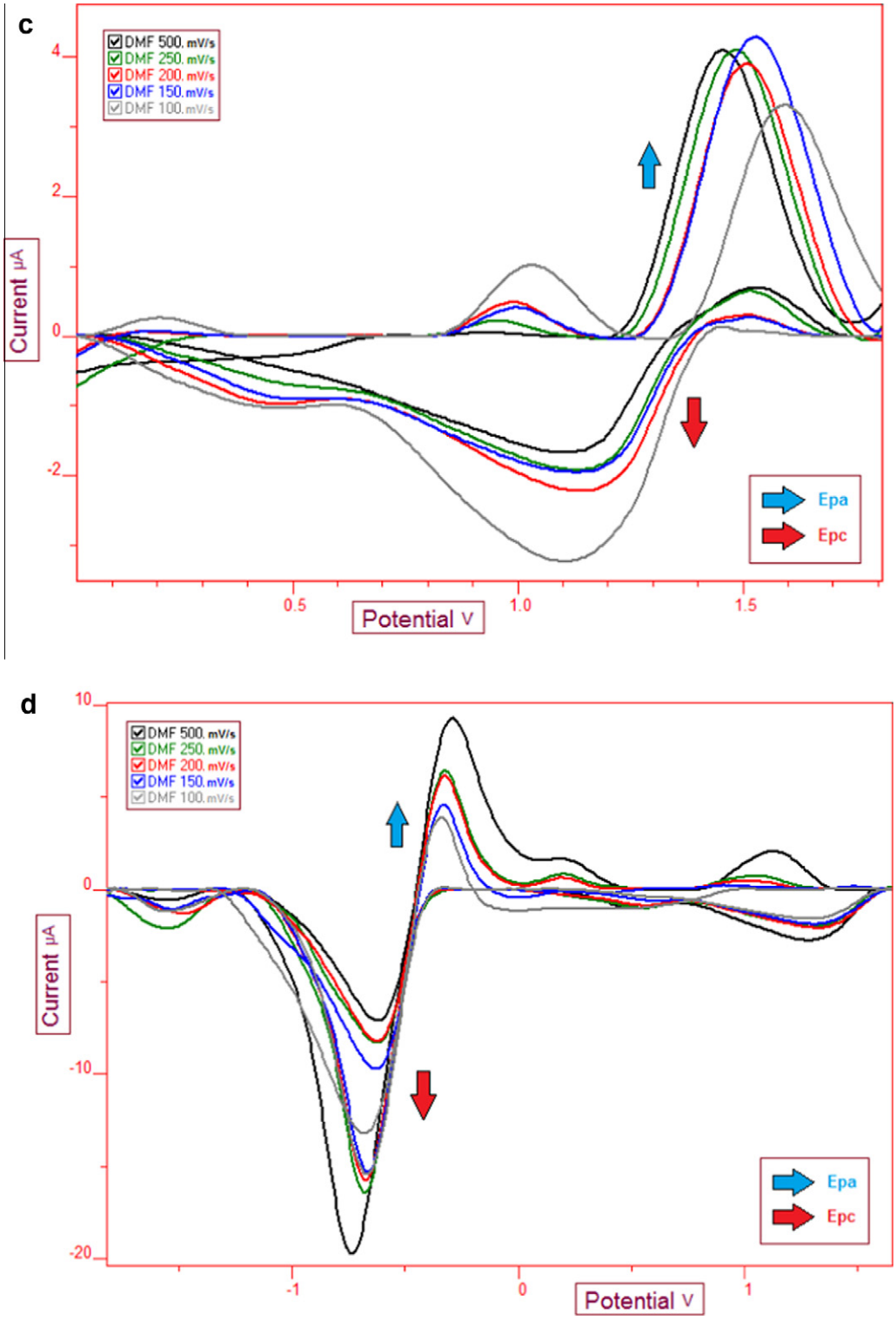


**Fig. 11** (*continued*)

the electrochemical response to the scan rate. In all cases, the anodic and cathodic peak potentials ($E_{pa}$ and $E_{pc}$) are relatively unchanged for scan rates of 100, 150, 200, 250 and 500 mV/s. However, the anodic and cathodic potential difference.

Schiff base ruthenium (III) complexes show two irreversible reduction wave ($\Delta E$ = 40–780 mV) on the negative side against $Ag^+$/AgCl, and two irreversible oxidation wave ($\Delta E$ = 80–590 mV) on the positive side. The former is assigned to Ru(III)/Ru(II) reduction and the latter is assigned to Ru(III)/Ru(IV) oxidation. The one-electron nature of these waves can be established by comparing the peak heights for each wave with that of the ferrocene–ferrocenium couple ($\Delta E$ = 40 mV, $\Delta E$ = −610 mV and $I_{pa}/I_{pc}$ = 0.98) under the same conditions. Similar results were reported for other octahedral ruthenium (III) complexes [27]. The effect of the

**Table 8**
Catalytic oxidation of cyclohexane (CyH) and cyclooctane with $H_2O_2$[a] under microwave irradiation[b].

| Catalyst | Substrate | CyH conversion (mol%) | Desired products (mol%) | ol:one | By products (mol%) |
|---|---|---|---|---|---|
| $Cu_2(L^1)(H_2O)_2(Cl)_2$ | CyH | 98.62 | Cy—OH (41.33); Cy=O (23.41) | 1.77 | 33.88 |
| | CyON | 63.44 | CyON—OH (2.84); CyON=O (14.30) | 0.20 | 46.30 |
| $Co_2(L^1)(H_2O)_2(Cl)_2$ | CyH | 98.20 | Cy—OH (13.92); Cy=O (6.57) | 2.12 | 77.71 |
| | CyON | 68.99 | CyON—OH (1.87); CyON=O (6.45) | 0.29 | 60.67 |
| $Cr_2(L^1)(H_2O)_4(NO_3)_4$ | CyH | 98.39 | Cy—OH (27.79); Cy=O (33.62) | 0.83 | 36.98 |
| | CyON | 70.12 | CyON—OH (6.99); CyON=O (32.35) | 0.22 | 30.78 |
| $Ru_2(L^1)(H_2O)_4(Cl)_4$ | CyH | 99.14 | Cy—OH (10.81); Cy=O (13.20) | 0.82 | 75.13 |
| | CyON | 72.07 | CyON—OH (3.67); CyON=O (11.40) | 0.32 | 57.00 |
| $Mn_2(L^1)(H_2O)_2(Cl)_2$ | CyH | 99.55 | Cy—OH (6.67); Cy=O (7.70) | 0.87 | 85.18 |
| | CyON | 72.27 | CyON—OH (2.00); CyON=O (11.20) | 0.18 | 59.07 |
| $Cu_2(L^2)(H_2O)_2(Cl)_2$ | CyH | 99.56 | Cy—OH (56.45); Cy=O (18.96) | 2.98 | 24.15 |
| | CyON | 71.08 | CyON—OH (2.64); CyON=O (12.75) | 0.21 | 55.69 |
| $Co_2(L^2)(H_2O)_2(Cl)_2$ | CyH | 99.70 | Cy—OH (4.29); Cy=O (1.16) | 3.70 | 94.25 |
| | CyON | 59.92 | CyON—OH (1.06); CyON=O (0.85) | 1.25 | 58.01 |
| $Cr_2(L^2)(H_2O)_4(NO_3)_4$ | CyH | 98.03 | Cy—OH (25.00); Cy=O (25.19) | 0.99 | 47.84 |
| | CyON | 77.94 | CyON—OH (7.77); CyON=O (24.95) | 0.31 | 45.22 |
| $Ru_2(L^2)(H_2O)_4(Cl)_4$ | CyH | 98.96 | Cy—OH (9.03); Cy=O (12.24) | 0.74 | 77.69 |
| | CyON | 64.18 | CyON—OH (2.66); CyON=O (9.00) | 0.30 | 52.52 |
| $Mn_2(L^2)(H_2O)_2(Cl)_2$ | CyH | 99.52 | Cy—OH (5.08); Cy=O (6.00) | 0.85 | 88.44 |
| | CyON | 67.57 | CyON—OH (0.72); CyON=O (3.90) | 0.18 | 62.95 |
| $Cu_2(L^3)(H_2O)_2(Cl)_2$ | CyH | 98.72 | Cy—OH (46.02); Cy=O (19.49) | 2.36 | 33.21 |
| | CyON | 79.37 | CyON—OH (2.65); CyON=O (11.40) | 0.23 | 65.32 |
| $Co_2(L^3)(H_2O)_2(Cl)_2$ | CyH | 99.86 | Cy—OH (2.88); Cy=O (0.72) | 4.00 | 96.26 |
| | CyON | 75.22 | CyON—OH (0.61); CyON=O (0.65) | 0.94 | 73.96 |
| $Cr_2(L^3)(H_2O)_4(NO_3)_4$ | CyH | 98.47 | Cy—OH (27.71); Cy=O (29.68) | 0.93 | 41.08 |
| | CyON | 74.86 | CyON—OH (6.05); CyON=O (30.65) | 0.20 | 38.16 |
| $Ru_2(L^3)(H_2O)_4(Cl)_4$ | CyH | 98.94 | Cy—OH (9.82); Cy=O (12.47) | 0.79 | 76.65 |
| | CyON | 60.97 | CyON—OH (3.44); CyON=O (11.60) | 0.30 | 45.93 |
| $Mn_2(L^3)(H_2O)_2(Cl)_2$ | CyH | 99.81 | Cy—OH (2.70); Cy=O (4.54) | 0.60 | 92.57 |
| | CyON | 64.28 | CyON—OH (0.27); CyON=O (0.90) | 0.30 | 63.11 |

[a] 0.02 mmol catalyst:2 mmol cyclohexane:3 mmol hydrogene peroxide (1:100:150) and 5 mL acetonitrile were used for each reaction.
[b] 400 W power were applied for 60 min. The reaction temperature and pressure were held at around 140 °C and 30 bar in closed DAP60 vessels.

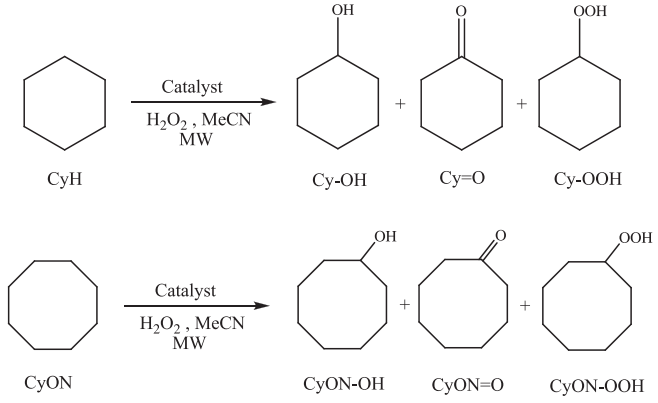


**Fig. 12.** Catalytic oxidation of cyclohexane and cyclooctane under microwave irradiation.

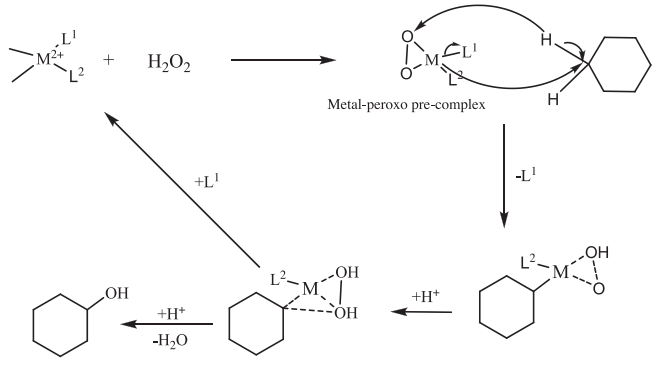


**Fig. 13.** Possible catalytic oxidation mechanism.

*para*-substituents (X) present in the Schiff base ligands is much more pronounced in the case of ruthenium (III)–ruthenium (IV) irreversible oxidation.

### 3.3. Cyclohexane and cyclooctane oxidation under microwave irradiation

In order to determine the optimum reaction conditions, the effects of the temperature, pressure, co-catalyst, reaction time and solvent on the cyclohexane and cyclooctane were investigated. The effect of the catalyst amount on oxidation at a temperature of 140 °C was studied. Although the conversion of cyclohexane and cyclooctane are nearly unchangeable with the increasing of the amount of catalyst, it is beneficial for the transformation of the cyclohexane and cyclooctane to the cyclic alcohols and ketones.

The decrease in the activity could be mainly attributed to the loss of metal atoms and catalyst during the reaction and filtration. From the average of the results, the activities of the Schiff base transition metal catalysts can be arranged in the following manner: Ru(III) < Mn(II) < Co(II) < Cr(III) < Cu(II). Metal complexes of the ligand $H_2L^2$ show the highest activity on the alkane oxidation compared to the metal complexes of other ligands. In the ligand $H_2L^2$, there is a hydroxyl group on the *p*-position in the salicylidene moiety. This group increases the π-electron density of the ring by the mesomeric effect. The optimized reaction conditions could be applied to the oxidation reaction of cyclohexane and cyclooctane by the Schiff base metal complexes as a catalyst and the obtained data are given in Table 8. The catalytic oxidation of alkanes with 30% $H_2O_2$ under mild reaction conditions is especially an interesting topic, because direct functionalization of inactivated C—H bonds in saturated hydrocarbons usually requires drastic reaction conditions, such as high pressure and temperature. The optimum

oxidation conditions were obtained as catalyst:substrate:oxidant ratio of 1:100:200 in acetonitrile under 400 W microwave power for 60 min. The temperature and pressure were controlled at about 140 °C and 30 bar by the instrument. A blank has been run under the same conditions without any catalyst. According to a possible oxidation mechanism, first and slow step is the oxidation of CyH and CyON to cyclic-alcohols and cyclic-ketones and other further oxidized products arise. If the first step is controlled, the selectivity of the desired products, Cy—OH, Cy=O from the substrate CyH and CyON—OH, CyON=O from the substrate CyON, can be increased. The obtained reaction products using $H_2O_2$ and catalyst under microwave irradiation are shown in Fig. 12.

A possible catalytic oxidation mechanism is given in Fig. 13. In this process, $H_2O_2$ is the oxidant, the metal complexes are the catalyst and the cyclohexanol forms as an intermediate product. The oxidation reactions come to pass around the metal of the complexes. It has been proposed that the microwave power and the novel catalysts could affect the selective oxidation of CyH to

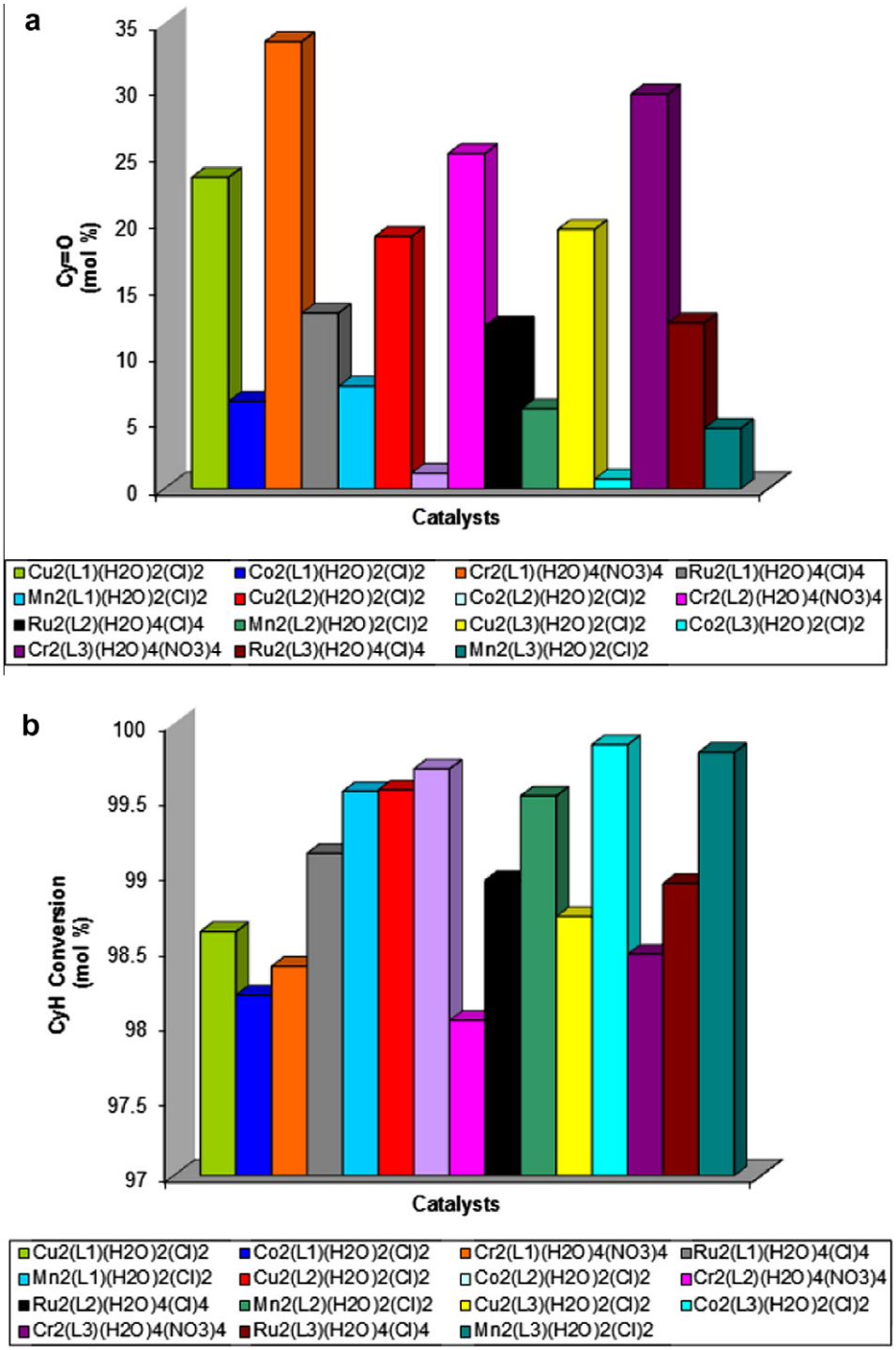


**Fig. 14.** Influence of the complexes in cyclohexane and cyclooctane oxidation under microwave irradiation. 0.02 mmol catalyst: 2 mmol cyclohexane (cyclooctane): 4 mmol hydrogene peroxide (1:100:200) and 5 mL acetonitrile were used for each reaction. 300 W power were applied for 30 min. The reaction temperature and pressure were held at around 100 °C and 30 bar in closed DAP60 vessels.

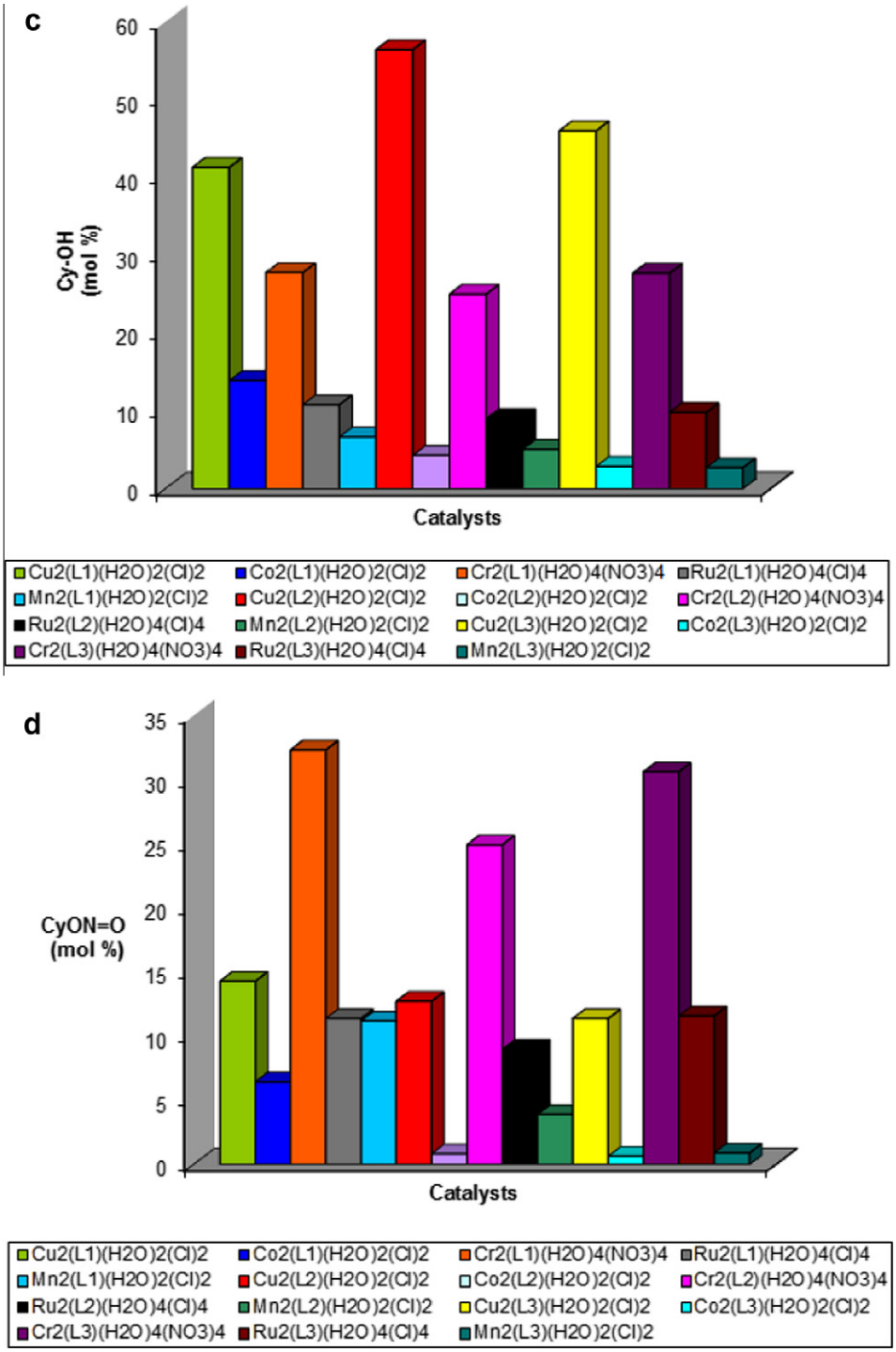


**Fig. 14** (*continued*)

Cy—OH, Cy=O and CyON to CyON—OH, CyON=O. The synthesized Cu(II) and Cr(III)complexes showed good catalytic activity in the oxidation of cyclohexane and cyclooctane, yielding the desired oxidized products. On the other hand, the Mn(II), Co(II) and Ru(III) complexes did not show good selective catalytic effect when compared to the literature data [11–17]. In all catalysis reactions examined, the Cu(II) and Cr(III) complexes have the highest catalytic activity compared to the other metal complexes for the selectivities of the desired products Cy—OH (cyclohexanol), Cy=O (cyclohexanone), CyON—OH (cyclooctanol), CyON=O (Table 8, Fig. 14).

In our study, the Co(II), Mn(II) and Ru(III) complexes showed low catalytic activity on the cyclohexane and cyclooctane substrates. The catalytic performance of the Cu(II) complexes may comparable to the activity exhibited by the earlier reported complexes [11,14]. The key point in the conversion of cyclohexane to the oxidized products is the reduction of M(II)–L to M(I)–L (L: ligand). This reduction to M(I)–L is facilitated the ligands available around the metal cation. The formation of the oxidation products Cy—OH and Cy O show the preferential attack of the activated bonds. Tetrahedral geometry of Cu(II) complex may be the reason of the having higher activity rather than the other complexes.

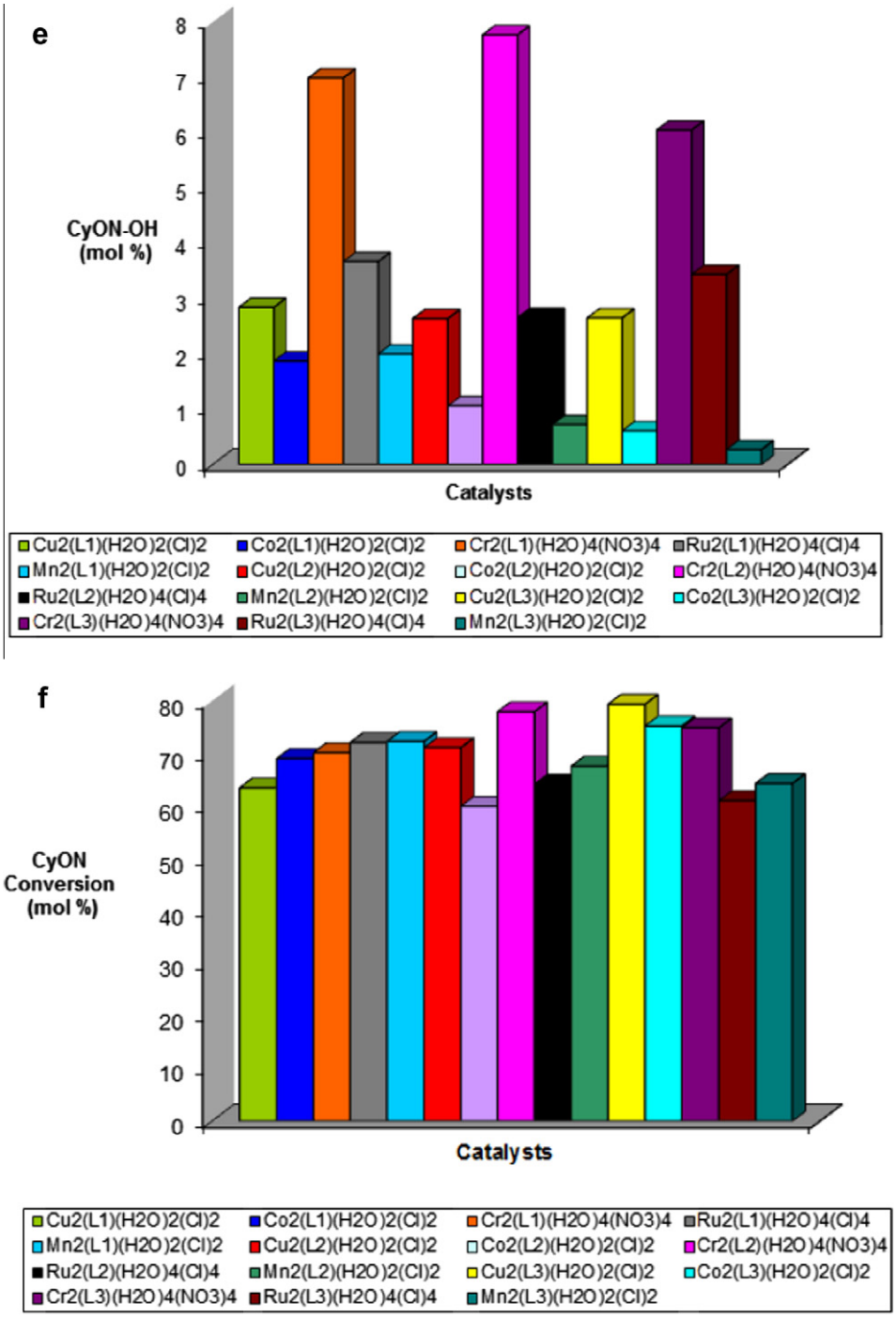


**Fig. 14** (*continued*)

In order to give more insight into the structure of the complexes, the thermal studies of the complexes have been carried out using thermogravimetry (TG-DTA) techniques. The thermogravimetric analyses for the ligands and metal complexes were carried out within the temperature range from ambient temperature up to 900 °C. The thermal curve of the $Cu_2(L^1)(H_2O)_2(Cl)_2$ complex is given in Fig. 15. The thermal behavior of all the complexes was almost the same. It was found from TG analysis that the binuclear metal complexes start losing mass in the 105–120 °C and end in the 480–670 °C temperature range after losing big part of total mass, but the decomposition did not finish completely at this temperature range. The examination of TG curves showed that the complexes decompose in least four or more stages. These decomposition steps correspond to loss of the coordinated $H_2O$ molecules, two/four Cl atoms, four nitrate groups and Schiff base ligands. Fourth step did not finish completely within the temperature range 670–880 °C.

## 4. Conclusion

In this paper, we obtained three Schiff base ligands ligands ($H_2L^1$–$H_2L^3$) and their Cu(II), Co(II), Ni(II), Mn(II) and Cr(III) complexes and investigated as analytical, spectroscopic, thermal and electrochemical. We obtained the ligand $H_2L^1$ and $H_2L^3$ as single

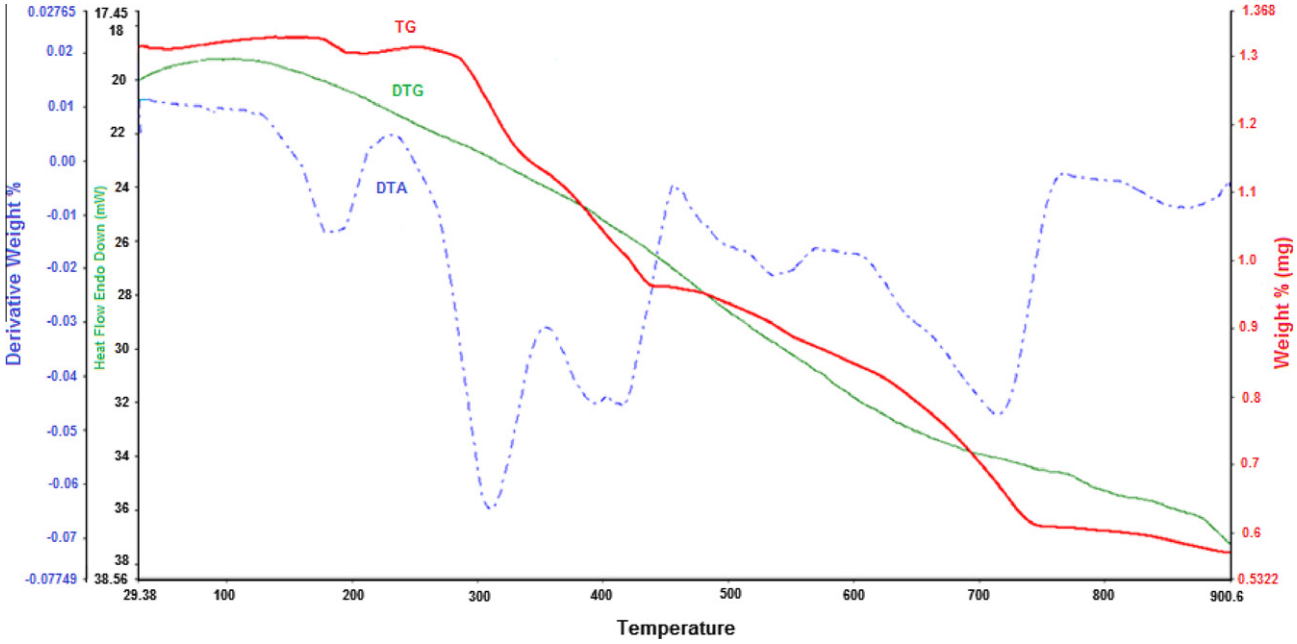


**Fig. 15.** The thermal curve of the $Cu_2(L^1)(H_2O)_2(Cl)_2$ complex.

crystals and investigated their structures by X-ray technique. We studied alkane oxidation reactions of the transition metal complexes using cyclohexane and cyclooctane as substrates. The Cu(II) and Cr(III) complexes showed good catalytic activity in the oxidation of cyclohexane and cyclooctane to the desired oxidized products.

## Acknowledgement

We are grateful to the Scientific & Technological Research Council of Turkey (TUBITAK) (Project No.: 109T071) for the support of this research.

## Appendix A. Supplementary data

Full crystallographic data for the reported ligands ($H_2L^1$ and $H_2L^3$) have been deposited with the Cambridge Crystallographic Data Center, CCDC Nos. 847259 and 856306, respectively. Copies of this information may be obtained by writing your request to: The Director, CCDC, 12 Union Road, Cambridge CB2 1EZ, UK (fax: +44 1223 336 033; e-mail: deposit@ccdc.cam.ac.uk or http://www.ccdc.cam.ac.uk).

## References

[1] T. Inabe, New J. Chem. 15 (1991) 129–136.
[2] M.Z. Zgierski, J. Chem. Phys. 115 (2001) 8351–8358.
[3] A. Filarowski, A. Koll, T. Glowiok, J. Chem. Soc. Perkin Trans. 2 (2002) 835–842.
[4] K.B. Borisenko, I. Hargittai, J. Mol. Struct. (THEOCHEM) 388 (1996) 107–113.
[5] T. Sekikawa, T. Kobayashi, T. Inabe, J. Phys. Chem. A 101 (1997) 644–649.
[6] B. Zheng, S. Brett, J.P. Tite, T.A. Brodie, J. Rhodes, Science 256 (1992) 1560–1563.
[7] D.A. Atwood, M.J. Harvey, Chem. Rev. 101 (2001) 37–52.
[8] C.M. Che, J.S. Huang, Coord. Chem. Rev. 242 (2003) 97–113.
[9] L. Canali, D.C. Sherrington, Chem. Soc. Rev. 28 (1999) 85–93.
[10] (a) V.C. Gibson, S.K. Spitzmesser, Chem. Rev. 103 (2003) 283–315; (b) G.J.P. Britovsek, V.C. Gibson, D.F. Wass, Angew. Chem. Int. Ed. 38 (1999) 428–447.
[11] B. Retcher, J.S. Costa, J. Tang, R. Hage, P. Gamez, J. Reedijk, J. Mol. Catal. A: Chem. 286 (2008) 1–5.
[12] S. Tanase, J. Reedijk, R. Hage, G. Rothenberg, Top. Catal. 53 (2010) 1039–1044.
[13] M.M.Q. Simoes, I.C.M.S. Santos, M.S.S. Balula, J.A.F. Gamelas, A.M.V. Cavaleiro, M.G.P.M.S. Neves, J.A.S. Cavaleiro, Catal. Today 91–92 (2004) 211–214.
[14] R. Luque, S.K. Badamali, J.H. Clark, M. Fleming, D.J. Macquarrie, Appl. Catal. A: Gen. 341 (2008) 154–159.
[15] S. Uruş, M. Dolaz, M. Tümer, J. Inorg. Organomet. Polym. 20 (2010) 706–713.
[16] M. Dolaz, V. McKee, S. Uruş, N. Demir, A.E. Şabik, A. Gölcü, M. Tümer, Spectrochim. Acta A. 76 (2010) 174–181.
[17] N.M.F. Carvalho, H.M. Alvarez, A. Horn Jr., O.A.C. Anutes, Catal. Today 133–135 (2008) 689–694.
[18] Bruker, APEX2 and SAINT Bruker AXS Inc., 1998.
[19] G.M. Sheldrick, Acta Cryst. A 64 (2008) 112.
[20] A. Gölcü, M. Tümer, H. Demirelli, R.A. Wheatley, Inorg. Chim. Acta 358 (2005) 1785–1797.
[21] M. Tümer, N. Deligonul, A. Gölcü, E. Akgün, M. Dolaz, H. Demirelli, M. Dığrak, Transition Met. Chem. 31 (2006) 1–12.
[22] M. Tümer, H. Köksal, S. Serin, M. Dığrak, Transition Met. Chem. 24 (1999) 13–17.
[23] M. Tümer, H. Köksal, S. Serin, Synth. React. Inorg. Met.-Org. Chem 28 (1998) 1393–1404.
[24] A.T. Çolak, F. Çolak, O.Z. Yeşilel, D. Akduman, F. Yılmaz, M. Tümer, Inorg. Chim. Acta 363 (2010) 2149–2162.
[25] A.B. Lever, Inorganic Electronic Spectroscopy, Elsevier, London, UK, 1980.
[26] A.A. Osowole, G.A. Kolawole, R. Kempe, O.E. Fagade, Synth. React. Inorg. Met.-Org. Chem. 39 (2009) 165–174.
[27] M. Tümer, E. Akgün, S. Toroğlu, A. Kayraldız, L. Dönbak, J. Coord. Chem. 61 (2008) 2935–2949.